A Fault Detection Scheme for Modeled and Unmodeled Faults in a Simple Hydraulic Actuator System Using an Extended Kalman Filter

---

A thesis presented to the faculty of the Graduate School
University of Missouri-Columbia

In Partial Fulfillment
Of the Requirements for the Degree
Master of Science

By

CODY RYERSON

Dr. Craig Kluever, Thesis Supervisor

AUGUST 2006

The undersigned, appointed by the dean of the Graduate School, have examined the project entitled

A Fault Detection Scheme for Modeled and Unmodeled Faults in a Simple Hydraulic Actuator System Using an Extended Kalman Filter

Presented by Cody Ryerson

a candidate for the degree of Masters of Science

and hereby certify that in their opinion it is worthy of acceptance.

Dr. Craig Kluever, Professor, Mechanical and Aerospace Engineering

Dr. Roger Fales, Assistant Professor, Mechanical and Aerospace Engineering

Dr. Steven Borgelt, Associate Professor, Biological Engineering

ACKNOWLEDGEMENTS

To date, my work in the graduate school at the University of Missouri-Columbia has been the most challenging period in my life; it has also been one of the most enjoyable. Upon entering graduate school, I was not sure what to expect. Now, it is the standard I compare other work experiences to. I am very proud of my work here at the university, but I cannot take all of the credit. I share my achievements with those around me who have given me constant support and encouragement.

I have written dozens of pages on this project alone, but I do not have the words to adequately express my thanks to my academic advisor, Dr. Craig Kluever. I thank him for his guidance, encouragement, and perhaps most importantly, his patience. Our work did not always go as planned over the past year and a half, but, thanks in large part to Dr. Kluever's support, we made it to the end.

I am also thankful to Dr. Roger Fales for his insight into all things hydraulic and for providing a different perspective as this project gradually took shape. I also thank him for agreeing to participate on my thesis committee.

I also owe thanks to Dr. Steven Borgelt for taking the time to serve on my committee.

And finally, there is no metric for evaluating the contributions from my family and friends. I can only say that I owe a debt of gratitude to my parents, Dave and Wendy, my brothers Ian and Tyler, and all of my other innumerable family, friends, colleagues, and peers who have aided me along the way.

TABLE OF CONTENTS

LIST OF FIGURES

LIST OF TABLES

NOMENCLATURE

Symbol	Description	Units
P_1	Cylinder chamber 1 pressure	Pa
P_2	Cylinder chamber 2 pressure	Pa
x	Cylinder piston position	m
$\dot{x}$	Cylinder piston velocity	m/s
y	Spool valve position	m
$\dot{y}$	Spool valve velocity	m/s
b	Cylinder viscous friction coefficient	N-s/m
β	Fluid bulk modulus	Pa
P_s	Supply pressure	Pa
P_r	Reservoir pressure	Pa
P_0	Atmospheric pressure	Pa
ζ	Damping ratio	-
ω_n	Natural frequency	rad/s
K_{sp}	Spool valve servomotor gain	m/mA
u	Input signal	ma
Q	Flow rate	m^3/s
Q_{leak}	Leaked flow rate	m^3/s
C_d	Discharge coefficient	-
A_v	Open valve area	m^2
ρ	Fluid density	kg/m^3
V	Cylinder chamber volume	m^3
$\dot{V}$	Change in cylinder chamber volume	m^3/s
A	Piston area	m^2
x_{min}	Fully retracted cylinder position	m
x_{max}	Fully protracted cylinder position	m
m	Piston mass	kg
F_c	Piston friction force	N
T_t	Truth simulation sample time	s
T_s	EKF sample time	s
P_k	Error covariance matrix	-
Φ_k	State transition matrix	-
V_k	Process noise matrix	-
K_k	Kalman gain matrix	-
C_k	Output matrix	-
W_k	Measurement noise matrix	-
$\hat{\mathbf{x}}$	State estimate vector	-

Symbol	Description	Units
$\mathbf{y}_m$	Measurement vector	-
σ	Standard deviation	-
σ^2	Covariance	-
k_{el}	External leakage coefficient	$m^3/s/Pa$
k_{il}	Internal leakage coefficient	$m^3/s/Pa$
$\boldsymbol{r}$	Error residual vector	-

ABSTRACT

In this work an extended Kalman filter (EKF) is used to detect a variety of faults in a simple hydraulic actuator system. The system includes a constant supply pressure feeding a spool valve, which controls a double-rod cylinder with no applied load. Much interest exists in detecting faults in their early stages in the hopes that machine downtime and repair costs can be kept to a minimum. This EKF model employs two different techniques for identifying the presence of system faults. In one case, parameters of interest are included in the state-space model as augmented states. Faults are then introduced into these new states, and the EKF successfully detects the faults by tracking the new post-fault parameter values. The second method is an indirect approach for identifying unmodeled faults. These faults become apparent through analysis of the difference between a state measurement and estimate, known as error residual data. It is shown that, for this simple hydraulic system, this extended Kalman filter detects system faults confidently and promptly.

Chapter 1

INTRODUCTION

Much interest is directed towards detecting a fault in its early states before high-cost damage occurs to reduce the cost of lost machine-hours and repairs due to fault-related damage in a fluid power system. This work describes a fault detection method for a hydraulic actuator system. An extended Kalman filter (EKF)-type state estimator is used here to detect a variety of hydraulic system faults.

1.1 Fault Detection Scheme

The EKF requires a state-space model of the system. State-space representation is typically the smallest number of physical variables that fully describe a system's behavior. In this case, there are six states: two cylinder chamber pressures, cylinder piston position and velocity, and valve position and velocity. The state-space model for this work will be augmented with two additional states, cylinder viscous friction coefficient and fluid bulk modulus, that previously were considered to be constant parameters. Estimates of two augmented states are compared to expected values for those parameters to determine the existence of a fault. A deviation in friction coefficient might indicate the presence of foreign substances in the system, general degradation of system materials, or even a major event altering the piston's alignment. Gross changes in fluid bulk modulus could indicate the presence of entrained air or some other contaminant in the hydraulic fluid.

The EKF directly estimates viscous friction coefficient and fluid bulk modulus to detect the presence of modeled faults by comparing the value of augmented states to expected ranges for each parameter for the course of a normal operation. However, leakages are identified indirectly. Changes in parameters that are not estimated (such as leakage coefficients) are reflected by changes in error residuals, which are the difference between a parameter's estimate and its measured value. This model assumes sensors are in place for three measurements: two cylinder chamber pressures and the piston position. Thus, error residual data are available for those three states. Some types of faults are more apparent in the residuals for particular states than in others. For example, leakages are more apparent from the pressure residuals than from the piston position residual. This EKF scheme can detect internal leakages across the cylinder from the high-pressure chamber to the low-pressure chamber, as well as external leaks from the chambers to atmosphere. Besides leakages, an examination of the error residual data should be capable of indicating the presence of any type of fault that is not modeled by the EKF.

1.2 Literature Survey

Fault detection in hydraulically actuated systems has drawn interest recently. The use of state observers in fault detection schemes has become especially common in the last five years. The work presented here draws much from two different recently published fault detection methods. The determination of unmodeled faults through the analysis of EKF error residual data is described in detail by An and Sepehri [1, 2]. Also, a direct fault detection method through the estimation of augmented states with an EKF is presented by Chinniah et. al [3]. Song and Sepehri [4] show a similar process of

detecting faults through the use of parametric estimation employing a standard state observer. The procedure described in this work attempts to combine these two fault detection schemes into one algorithm. State estimators have become common for the application of fault detection. Shields et. al [5] describe a general overview of fault detection observers for nonlinear systems. The decision to use an EKF-type state observer for this work was influenced by its strong track record in fault detection systems in a wide range of applications, including, but not limited to, hydraulic actuators. For example, Hagiyev and Caliskan [6] successfully demonstrated the use of a Kalman to detect faults in flight control systems. A collection of various fault detection techniques is provided by Venkatasubramanian et. al [7]. Frank [8] discusses the effect of system uncertainty on an observer-based fault detection system. While state observers are commonly used in fault detection systems, there are some alternative approaches. An analytical redundancy (AR) approach is used by Chow and Willsky [9]. For yet another method for detecting faults, De Parsis and Isidori [10] discuss a purely geometric technique. It is clear there are numerous fault detection techniques available, each offering different advantages over other methods.

1.3 Thesis Outline

Chapter 2 describes the system model and presents the equations of motion. Additionally, the 2nd-order Euler integration method for state propagation is provided. Chapter 3 illustrates the EKF algorithm. Its equations and propagation loop are described, as well as its background and advantages for use as an on-site estimator for fault detection. In Chapter 4, the EKF model is verified against the true simulation. Also

described in this chapter is how the EKF error bounds from its error covariance matrix serve as a self-diagnostic tool for the filter. Chapter 5 presents the fault detection algorithm. First, the augmented states (cylinder viscous friction coefficient and fluid bulk modulus) are directly estimated to determine the presence of faults modeled by the EKF. Also, unmodeled faults, in the form of external and internal leakages, are detected by the EKF indirectly through the use of error residual data from the three measured states. Finally, Chapter 6 presents a summary of this fault detection method and approach, the overall conclusions of the results shown in this work, and potential future work to expand this research.

Chapter 2

SYSTEM MODEL

2.1 System Overview

The hydraulic system used for this examination is a simplified version of a desktop rig hydraulic actuator system used by An and Sepehri [1], which has been scaled to the approximate physical size of the Caterpillar 320c Excavator. The model is composed of a double-rod actuator controlled by a spool valve, shown in Fig. 2.1.1.

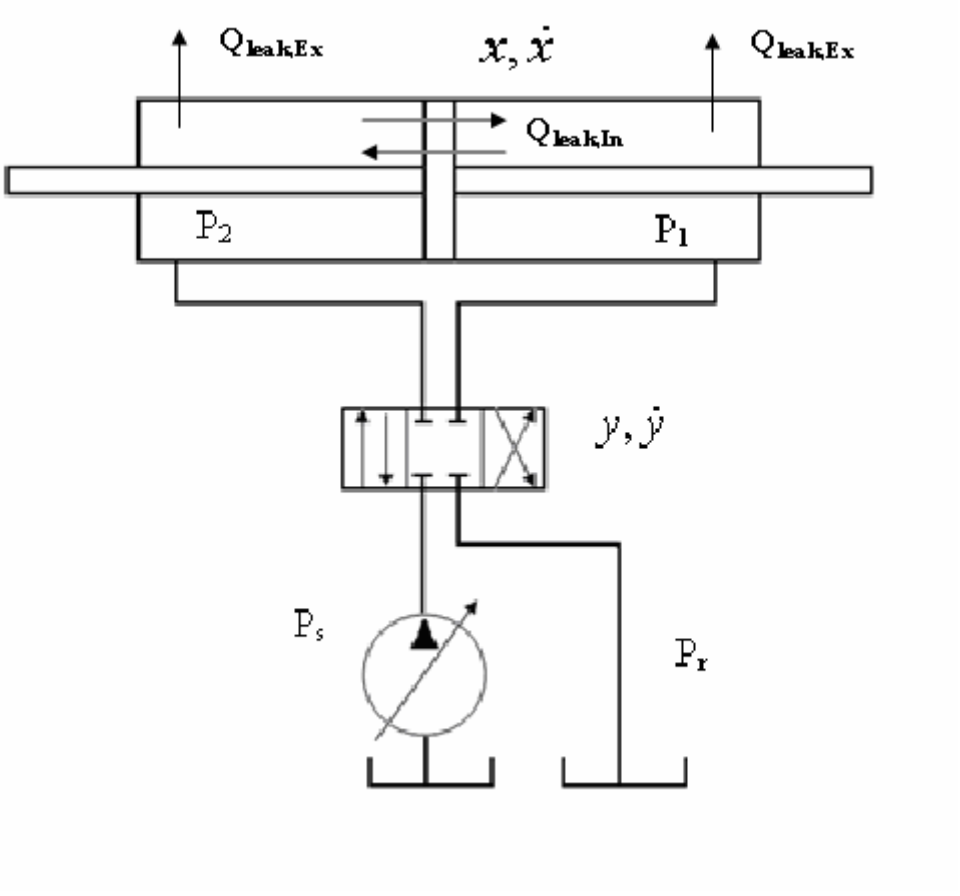

Fig. 2.1.1 – Schematic of the hydraulic actuator system

2.2 Equations of Motion

The spool valve dynamics are characterized by the following second-order equation:

$$\ddot{y} + 2\zeta\omega_n \dot{y} + \omega_n^2 y = K_{sp}\omega_n^2 u \tag{2.2.1}$$

where y is the valve position, u is the input signal, ω_n is the natural frequency, ζ is the damping ratio, and K_{sp} is the gain for the valve electromechanical servomotor. The input signal used for the simulations presented here is a sinusoid with a 2 second period, so the frequency is 0.5 Hz. The valve position determines the volumetric flow rate, Q, through the valve.

$$y > 0 \qquad \begin{cases} Q_1 = C_d A_v \sqrt{\dfrac{2}{\rho}(P_s - P_1)} \\ Q_2 = C_d A_v \sqrt{\dfrac{2}{\rho}(P_2 - P_r)} \end{cases} \tag{2.2.2}$$

$$y < 0 \qquad \begin{cases} Q_1 = C_d A_v \sqrt{\dfrac{2}{\rho}(P_1 - P_r)} \\ Q_2 = C_d A_v \sqrt{\dfrac{2}{\rho}(P_s - P_2)} \end{cases} \tag{2.2.3}$$

The pressure is given by P, C_d is the discharge coefficient, A_v is the open valve area, which is a function of valve position, and ρ is fluid density. Subscripts '*1*' and '*2*' denote the two pressure chambers, and subscripts '*s*' and '*r*' denote 'supply' and 'reservoir' values for pressure, respectively. P_s and P_r are both considered to be constants for this system.

The effect on the cylinder pressures from the flow through the valve is characterized by the pressure rise-rate equation:

$$\dot{P}_1 = \frac{\beta}{V_1}\left(Q_1 - \dot{V} - Q_{1,Leak}\right)$$
$$\dot{P}_2 = -\frac{\beta}{V_2}\left(Q_2 - \dot{V} - Q_{2,Leak}\right) \tag{2.2.4}$$

where β is the fluid bulk modulus, V is chamber volume described in Eq. (2.2.5), and Q_{Leak} is the leaked flow from the chamber (internal or external). Unless otherwise noted, Q_{Leak} is nominally zero. The rate of change of V depends on the piston area A and the piston velocity.

$$\begin{cases} V_1 = V_0 + A(x - x_{\min}) \\ V_2 = V_0 + A(x_{\max} - x) \end{cases} \tag{2.2.5}$$

$$\dot{V} = A\dot{x} \tag{2.2.6}$$

V_0 is the volume of hydraulic fluid in the supply lines, and x_{min} and x_{max} are the minimum and maximum piston positions, respectively.

The following equation shows the piston dynamics, derived using a force balance on the piston with no applied load:

$$\ddot{x} = \frac{1}{m}\left[\left(P_1 - P_2\right)A - F_c\right] \tag{2.2.7}$$

where x is piston position, m is piston mass, and F_c is the friction force on the piston, which is given by

$$F_c = b\dot{x} \tag{2.2.8}$$

This is a simple linear viscous friction model, with b as the friction coefficient.

2.3 State Propagation

Equations (2.2.1-2.2.6) can be converted to state-space representation to obtain the following six state model, which will be used as the baseline model for this project. The state vector is

$$\mathbf{x} = [P_1, P_2, x, \dot{x}, y, \dot{y}]^T \tag{2.3.1}$$

These states are integrated using a modified second-order Euler integration technique, which is shown in the following two equations:

$$\mathbf{x}^*_{k+1} = \mathbf{x}_k + \dot{\mathbf{x}}_k T_t \tag{2.3.2}$$

$$\mathbf{x}_{k+1} = \frac{1}{2}\left(\mathbf{x}_k + \mathbf{x}^*_{k+1} + \mathbf{x}^*_{k+1} T_t\right) \tag{2.3.3}$$

The subscript *k* denotes the current step, and *k+1* indicates the state at the next subsequent step. The superscript (*) represents an intermediate value used for the second Euler integration step. The sample time for the truth simulation, T_t, is 1 ms. The values for all of the parameters described in this chapter can be found in Table 2.3.1. These parameters are chosen to reflect the hydraulic system used for the bucket circuit on the Caterpillar 320c excavator.

Table 2.3.1 – System model parameter values.

Parameter	Value
Damping ratio (ζ)	0.733
Natural frequency (ω_n)	30 rad/s
Spool valve servomotor gain (K_{sp})	10^{-3} m/mA
Flow coefficient (C_d)	0.62
Density (ρ)	850 kg/m^3
Supply pressure (P_s)	10^6 Pa
Reservoir pressure (P_r)	$101(10^3)$ Pa
Fluid bulk modulus (β)	$1.57489(10^9)$ Pa
Supply line volume (V_0)	$2.2295(10^{-3})$ m^3
Piston area (A)	$8.422(10^{-3})$ m^2
Piston mass (m)	766 kg
Viscous friction coefficient (b)	17,000 N-s/m

Chapter 3

EXTENDED KALMAN FILTER

3.1 Background

The Kalman filter (KF) is a recursive state estimator developed by R.E. Kalman in 1960. A variation of the KF, called the extended Kalman filter (EKF) is used here. The EKF differs from the standard KF in one aspect: the KF assumes a linear system, while the EKF requires a system linearization with each step. Because much literature exists thoroughly describing the derivation of the Kalman filter, only the final equations and a brief description is presented here. The EKF, just like the basic KF, is made up of two stages; first, the EKF parameters for the next iteration are predicted, then the parameters are corrected using the update equations.

3.2 EKF Equations

The *a priori* state estimate, $\hat{\mathbf{x}}^{-}$, is predicted ahead using the single-step Euler integration routine. The over-hat (^) indicates the variable is an estimate, and the superscript (-) denotes the best estimate before correcting for the current state measurement. The EKF Euler integration step has a different sample time, T_s, which is 10 ms.

$$\hat{\mathbf{x}}_{k+1}^{-} = \hat{\mathbf{x}}_k + \dot{\hat{\mathbf{x}}}_k T_s \tag{3.2.1}$$

An initial guess for the state estimate, $\hat{\mathbf{x}}(0)$, is required from the user to start the EKF loop. $\dot{\hat{\mathbf{x}}}_k$ is a vector of the nonlinear right-hand side of the state-space model, and is a function of the previous state estimate and the user input, as seen in Eq. (3.2.2).

$$\dot{\hat{\mathbf{x}}} = \mathbf{f}[\hat{\mathbf{x}}, \mathbf{u}] \tag{3.2.2}$$

The initial state estimates can be seen in Table 4.1.1. The other step comprising the prediction stage is the projection for the error covariance matrix, P^-:

$$P_{k+1}^- = \Phi_k P_k \Phi_k^T + V_k \tag{3.2.3}$$

V_k is the process noise covariance matrix, which can be manually "tuned" to improve tracking, and Φ_k is the discrete state transition matrix (STM), which is the discrete Jacobian matrix of the nonlinear state equations.

$$\Phi_k = I + \frac{\partial \mathbf{f}}{\partial \mathbf{x}} T_s + \left(\frac{\partial \mathbf{f}}{\partial \mathbf{x}} \right)^2 \frac{T_s^2}{2!} + \ldots \tag{3.2.4}$$

Only the first two terms of Eq. (3.2.4) are used, as all additional terms have a negligible effect.

After the next values for the state estimate and error covariance matrix are predicted, the Kalman gain matrix, *K*, state estimate, and error covariance terms are updated, as seen in Eqs. (3.2.5-3.2.7). The KF is considered an *optimal* state estimator because the gain matrix *K* is formulated such that it minimizes the diagonal terms of the error covariance matrix for the next step.

$$K_k = P_k^- C_k^T \left(C_k P_k^- C_k^T + W_k \right)^{-1} \tag{3.2.5}$$

$$\hat{\mathbf{x}}_k = \hat{x}_k^- + K_k \left(\mathbf{y}_{m,k} - C_k \hat{\mathbf{x}}_k^- \right) \tag{3.2.6}$$

$$P_k = \left(I - K_k C_k \right) P_k^- \tag{3.2.7}$$

W_k is the measurement noise matrix, which is determined by sensor specifications and shown in Eq. (3.2.9), $\boldsymbol{y}_m$ is the new vector of measurements (P_1, P_2, x), and C_k is the output matrix from the state space formulation, which is shown in the following equation:

$$C_k = \begin{bmatrix} 1 & 0 & 0 & 0 & 0 & 0 \\ 0 & 1 & 0 & 0 & 0 & 0 \\ 0 & 0 & 1 & 0 & 0 & 0 \end{bmatrix} \tag{3.2.8}$$

$$W_k = \begin{bmatrix} (1kPa)^2 & 0 & 0 \\ 0 & (1kPa)^2 & 0 \\ 0 & 0 & (1mm)^2 \end{bmatrix} \tag{3.2.9}$$

W_k is a diagonal matrix containing the variances (σ^2) of the sensors. It is important to recognize that these are the squares of standard deviations, because, for a Gaussian distribution, about 68% of the data will exist between $\pm 1\sigma$ from the mean, which is zero. So, by Eq. (3.2.9), the pressure transducers for both of the cylinder chambers have a measurement accuracy of 1 kPa, and the piston position sensor has an accuracy of 1 mm.

The EKF equations form a recursive loop providing a current state estimate at each time step. Because this loop only requires the previous step's information, data storage is not needed. This makes the EKF ideal for "on site" type applications where large memory storage is unavailable or inconvenient. The KF loop can be seen in Fig. 3.2.1 [11]. Notice the discrepancy between Eq. (3.2.1) and the state estimate projection depicted in the figure. The equation in the figure, which uses the state transition matrix to project ahead in time for the next step, is a more general formulation of the EKF loop, which assumes a linear model. This approach prefers to use the nonlinear right-hand side equations and a first-order Euler integration step to project the state estimate forward in time.

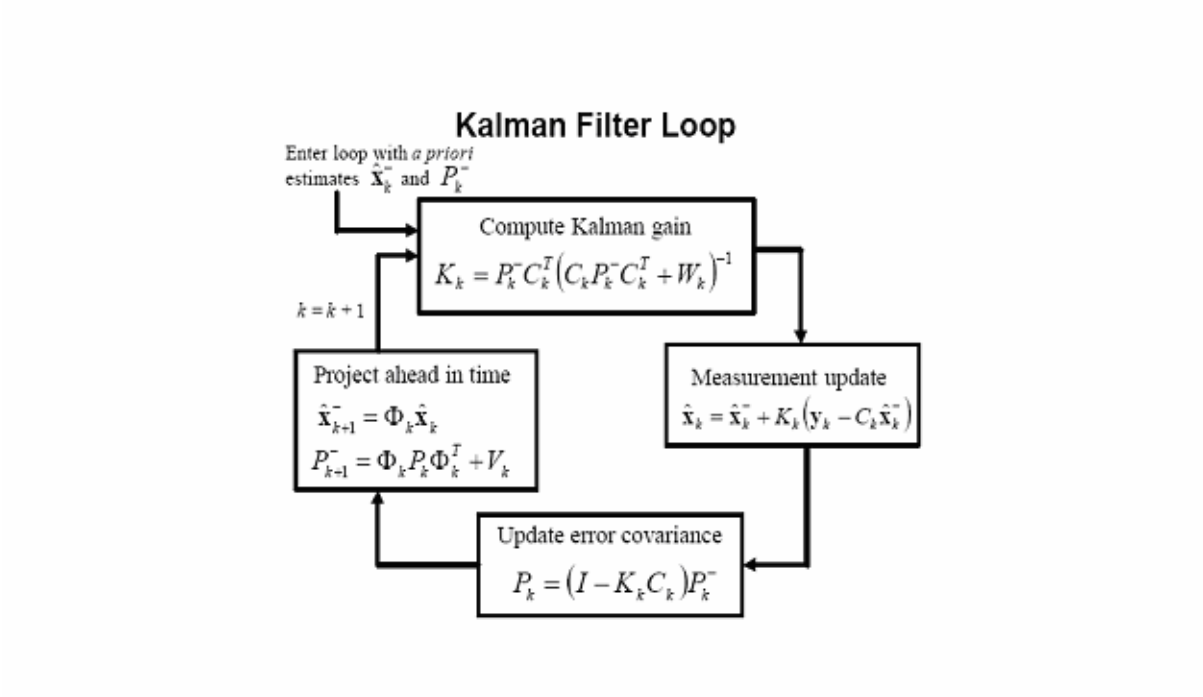

Fig. 3.2.1 Recursive Kalman filter loop

3.3 EKF Uncertainty Model

The measurement noise, process noise, and error covariance matrices are very important to the EKF model because, together, they describe the model uncertainty. The sensor accuracy, W_k, tempers the Kalman gain matrix. If the sensors are excessively noisy, then the gain matrix becomes smaller. The EKF is less aggressive in correcting for the deviation between measurement and estimate if it has less confidence in the measurement itself. The process noise covariance matrix, V_k, is a less intuitive quantity. It is a diagonal matrix containing each state's contribution to the overall uncertainty of the model. If the preferred level of performance is not achieved, the user can manually adjust these values to improve results. V_k directly contributes to the error covariance matrix, P_k, as seen in Eqs. (3.2.2) and (3.2.6). The error covariance matrix is extremely useful as a constantly updating diagnostic tool for the filter itself. The diagonal terms of

P_k will be used to measure the filter performance in tracking the states. Before entering the EKF loop, an initial guess for P_k is required from the user, then the matrix evolves with each new estimate. The process noise matrix, V_k, as well as the initial user input for P_k, can be found in the appendix.

Chapter 4

EKF MODEL VERIFICATION

4.1 State Tracking

In order for the EKF to confidently detect faults, the performance on the baseline nominal system must first be checked to ensure it is properly tracking the states. The tracking for all six states will be shown for this trial, but throughout the rest of this report, for the sake of brevity, only the relevant plots or enough plots to demonstrate the EKF performance will be shown. The initial conditions for both the truth simulation and the EKF state estimate are shown in Table 4.1.1.

Table 4.1.1 – Initial conditions for EKF loop.

State	True Value	Estimate
P_1	$8(10^6)$ Pa	$5(10^6)$ Pa
P_2	$8(10^6)$ Pa	$5(10^6)$ Pa
x	0.45 m	0
$\dot{x}$	0	0
y	0	0
$\dot{y}$	0	0

The state estimates are arbitrarily chosen with only the intention of being near the unknown true initial condition. For this simulation, the two cylinder chamber pressures, P_1 and P_2, are both taken to be half of the supply pressure, P_s. The other four estimates

are zero, implying a neutral starting condition. This simulation, as well as all others in this work, receives a 0.5 Hz sinusoidal input signal.

The true value and the EKF estimate are shown for all six of the physical states in Figs. 4.1.1-4.1.6. It should be noted that all of the states exhibit the same periodicity as the input signal. Ideally, there should be no discernible difference between the state estimate and the true state. It can be seen from these six plots that, at least by casual inspection, the EKF is tracking well. Obviously the estimate is not perfectly matched to the true state value. Figure 4.1.7 displays an enlarged view of a region of P_1 that exhibits chatter, which is the most difficult portion of the state to track, and it can be seen that the deviation between the estimate and the true value is insignificant for the purposes of state estimation. So it appears that, even "under the microscope," the EKF is performing soundly.

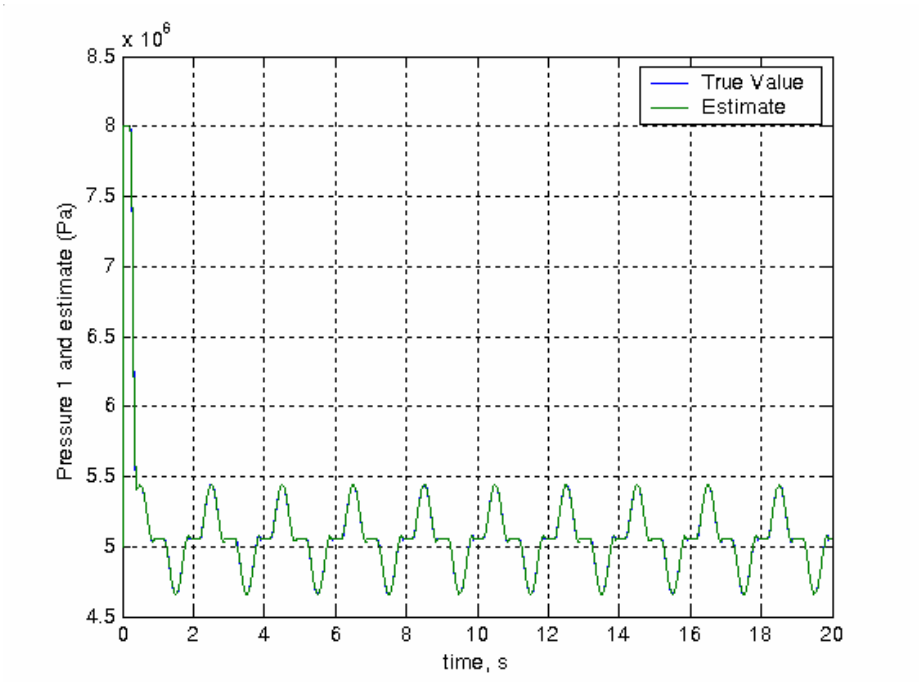

Fig. 4.1.1 Pressure 1 – True value and estimate (6-state EKF, nominal simulation)

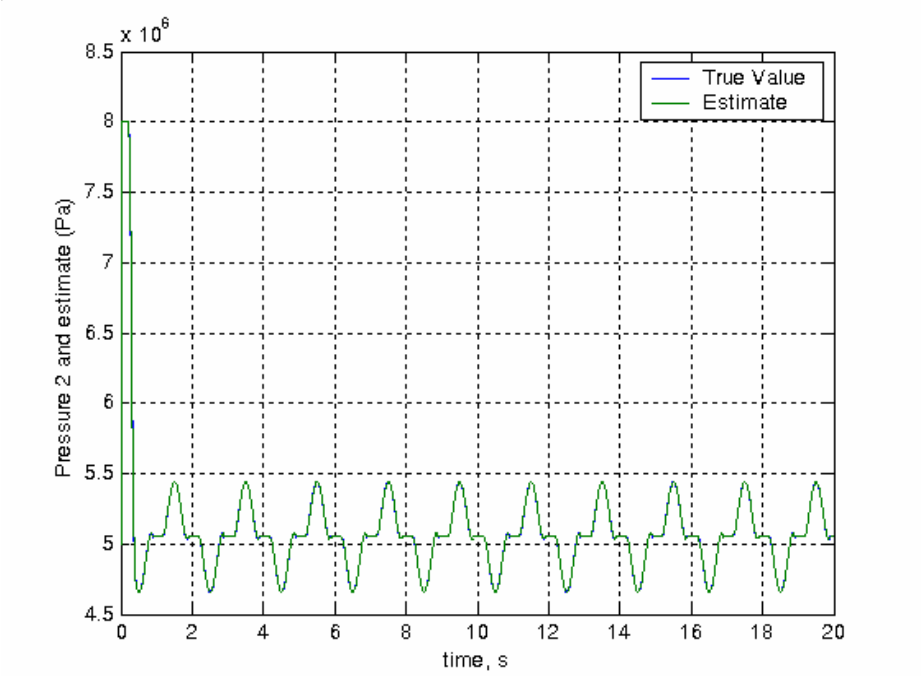

Fig. 4.1.2 Pressure 2 – True value and estimate (6-state EKF, nominal simulation)

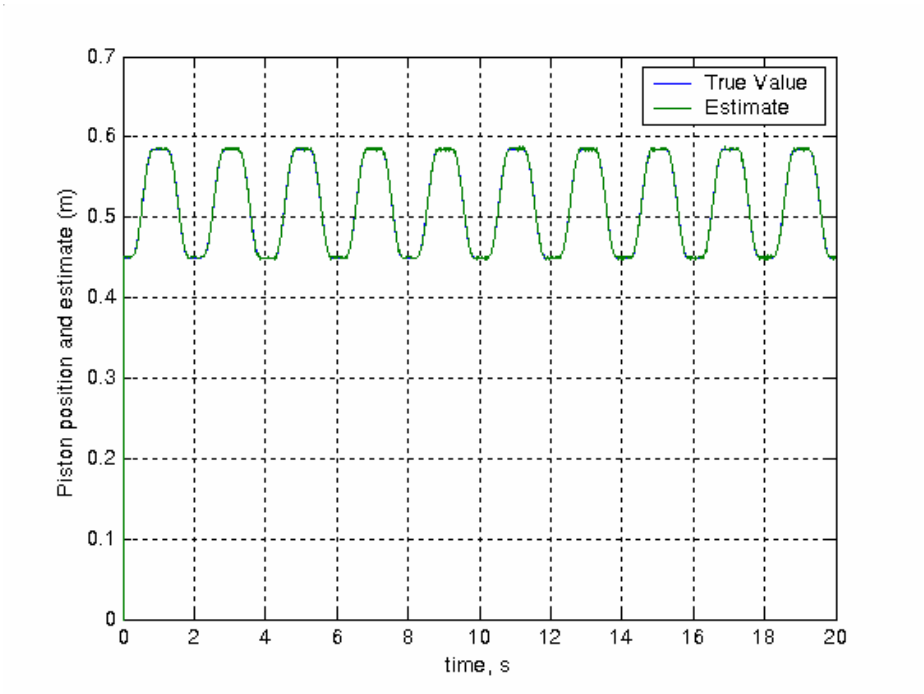

Fig. 4.1.3 Piston position – True value and estimate (6-state EKF, nominal simulation)

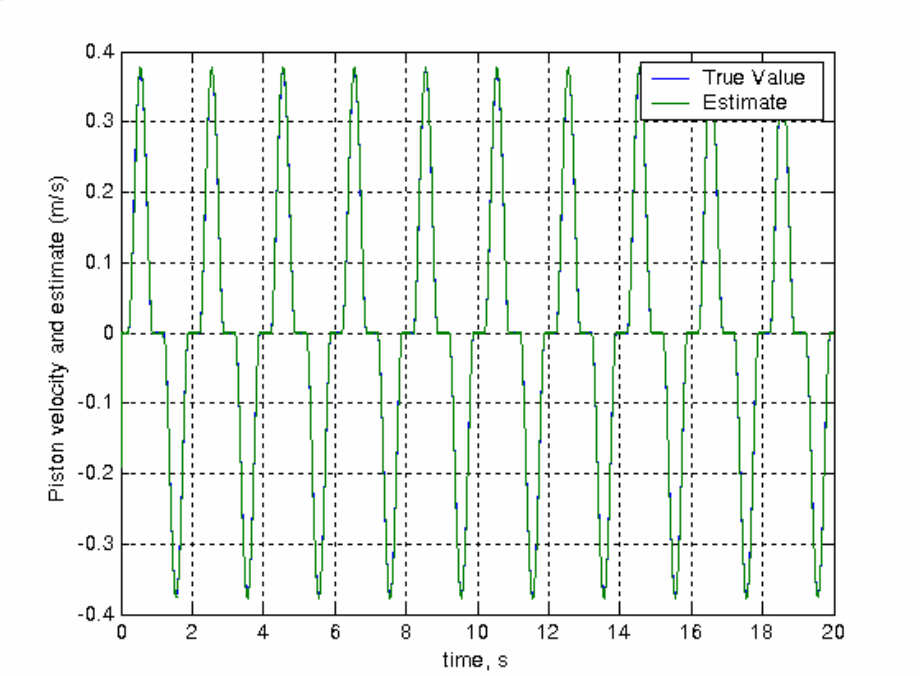

Fig. 4.1.4 Piston velocity – True value and estimate (6-state EKF, nominal simulation)

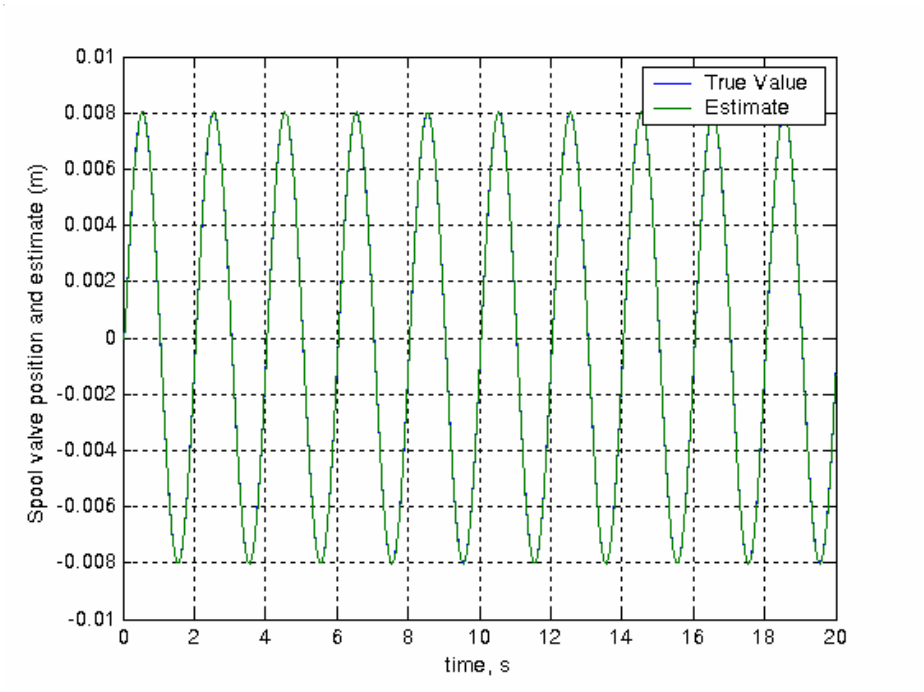

Fig. 4.1.5 Spool valve position – True value and estimate (6-state EKF, nominal simulation)

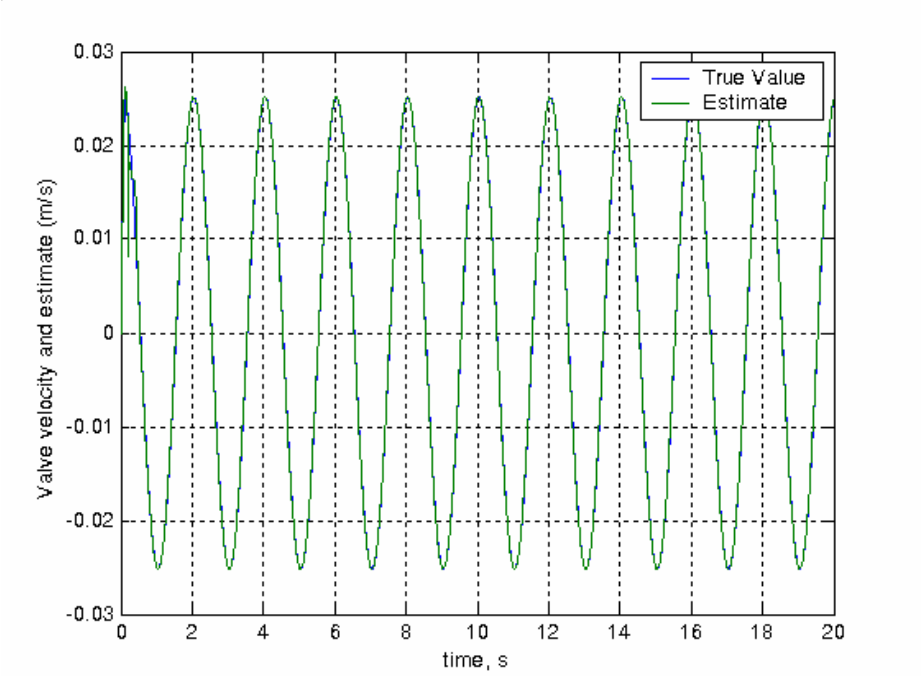

Fig. 4.1.6 Spool valve velocity – True value and estimate (6-state EKF, nominal simulation)

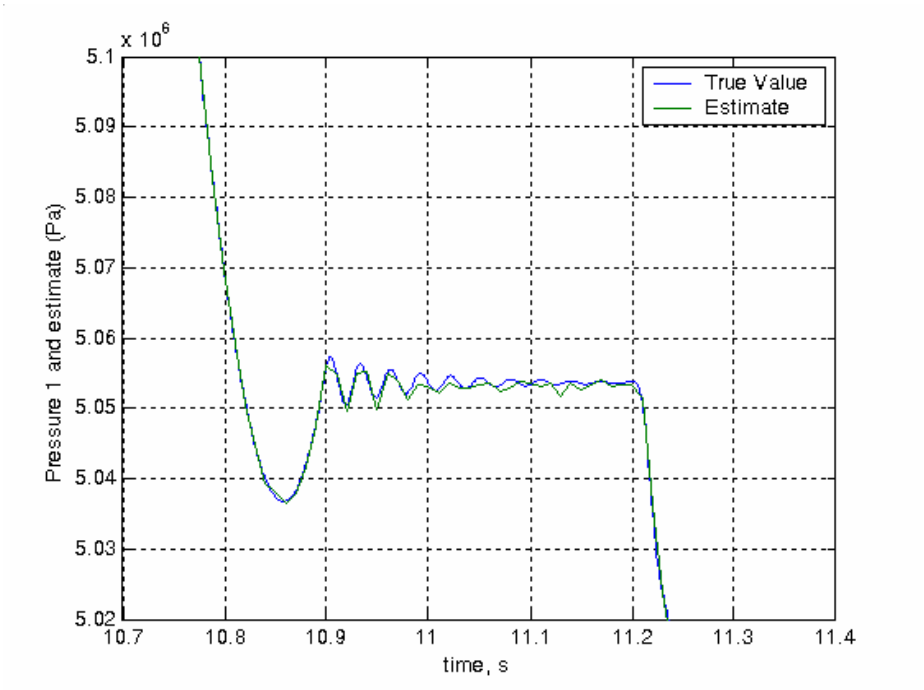

Fig. 4.1.7 Pressure 1 – Close-up view of true value and estimate (6-state EKF, nominal simulation)

4.2 EKF Error Bounds

In addition to being able to check state estimates by inspection, the EKF includes its own diagnostic tool. The diagonal terms of the error covariance matrix P_k provide 1-σ error bounds for state estimates. These error bounds provide a check of the filter's accuracy. If the EKF is performing correctly, about 68% of the estimation error signal should lie within the error bounds. This diagnostic is based on the standard deviation of a normally distributed random process, which is the structure of the uncertainty and noise matrices. It should be noted that the ±1-σ error bounds for P_1 in Fig. 4.2.1 are near 1 kPa. This is an artifact of the measurement accuracy for the pressure transducer used in the measurement noise matrix, W_k, which was assumed to also be 1 kPa, seen in Eq. (3.2.8). Similarly, the measurement accuracy for the piston position sensor has an accuracy of 1 mm, and the ±1-σ error bounds for piston position, x, in Fig. 4.2.2 are close to 1 mm. By inspection of Figs. 4.2.1 – 4.2.3, it can be seen that at least 68% of the estimation error signal falls within the ±1-σ error bounds, so it appears that the filter is indeed tracking well.

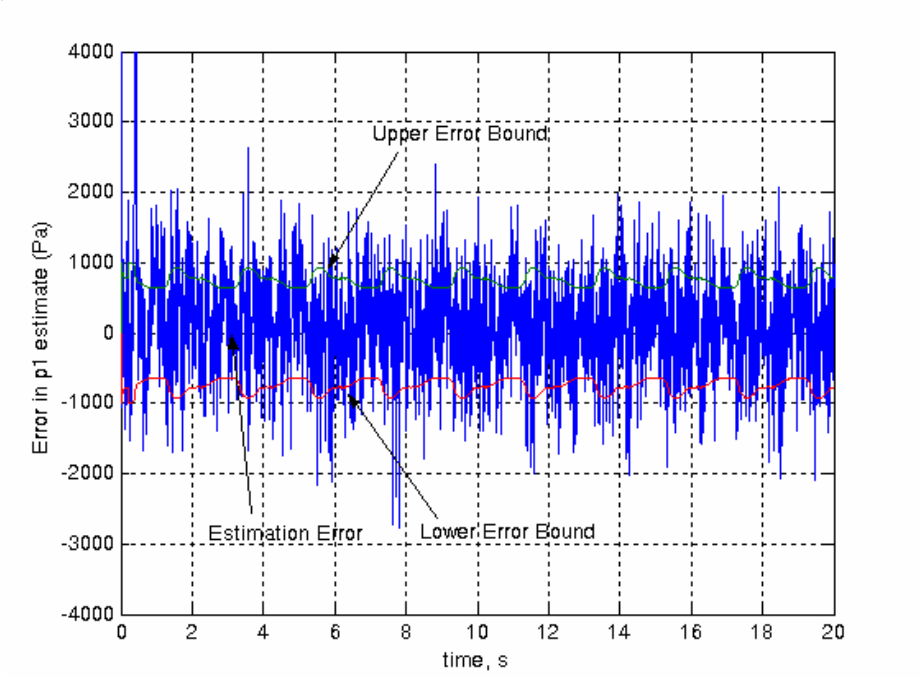

Fig. 4.2.1 Pressure 1 estimate error and error bounds (6-state EKF, nominal simulation)

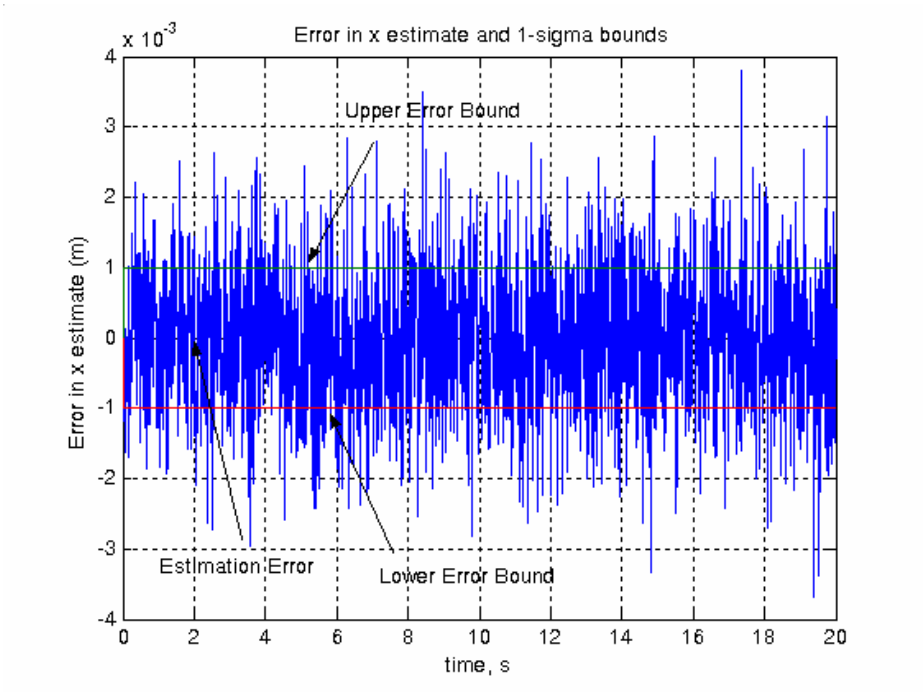

Fig. 4.2.2 Piston position estimate error and error bounds (6-state EKF, nominal simulation)

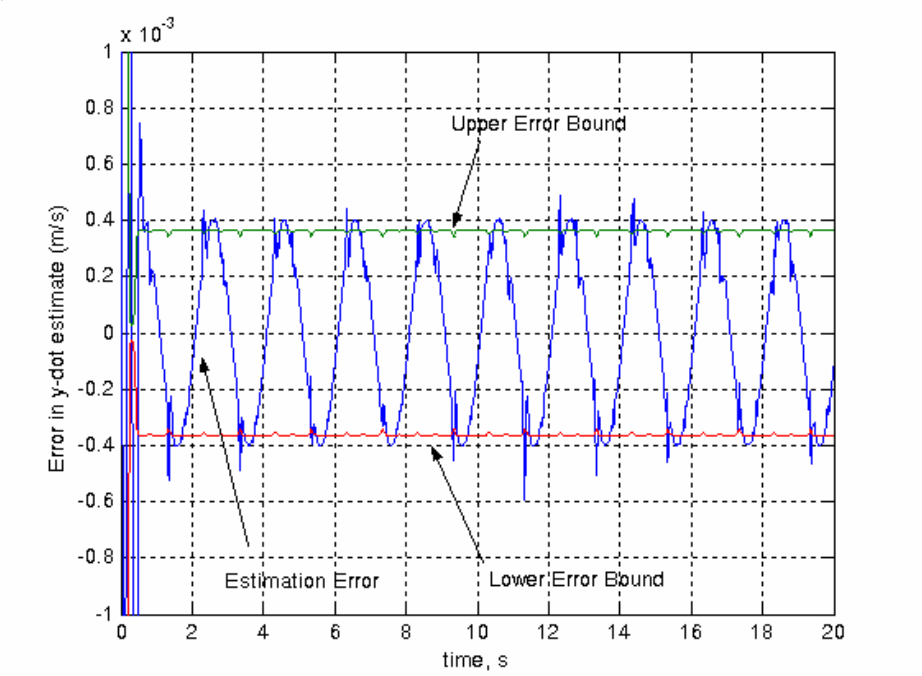

Fig. 4.2.3 Spool valve velocity estimate error and error bounds (6-state EKF, nominal simulation)

Chapter 5

FAULT DETECTION

5.1 Fault Detection Scheme

The six states estimated by the EKF up to this point are the minimum number of physical states necessary to fully describe the hydraulic actuator's dynamics. Additional "augmented states" will now be added to the EKF model, enabling the filter to track changes in those new states, as well as the original six. These augmented states already appear in the state-space representation, but are considered constant parameters. Indeed, if no fault occurs, these parameters will likely behave as constants throughout the course of system operation. A fault will be introduced into the truth simulation and if the EKF fault detector is performing properly, that fault will be reflected non-constant behavior for the estimates of the augmented states.

5.2 Viscous Friction Coefficient

The first augmented state is viscous friction coefficient, b, shown in Eq. (2.2.8), and is now the seventh state. Before introducing any faults, it is prudent to check the accuracy of the state estimates with this new augmented state added. Figure 5.2.1 shows that, after a brief time when the estimate is bad, the EKF manages to track the constant friction coefficient very well. The brief transient phase where the estimate is poor for approximately the first second of the simulation is due to the lack of knowledge the EKF has of the initial conditions of the true system model. Recall from Table 4.1.1 that the filter does not know the initial conditions of the truth model, it only requires a guess in

the "ballpark range" for each state. The same is true for viscous friction coefficient; for this simulation, the nominal value for b is 17,000 N-s/m (constant) and the initial state estimate, $\hat{b}(0)$, is assumed to be 10,000 N-s/m. The estimation plot in Fig. 5.2.1 and the error bounds found in Fig. 5.2.2 support the statement that the filter is accurately tracking, with at least 68% of the estimation error signal falling within the ±1-σ error bounds. It is also worth noting that adding a seventh augmented state to the EKF does not degrade the estimates of any of the other six classic states. As an example, the data from the first state, P_1, is presented in Figs. 5.2.3 and 5.2.4.

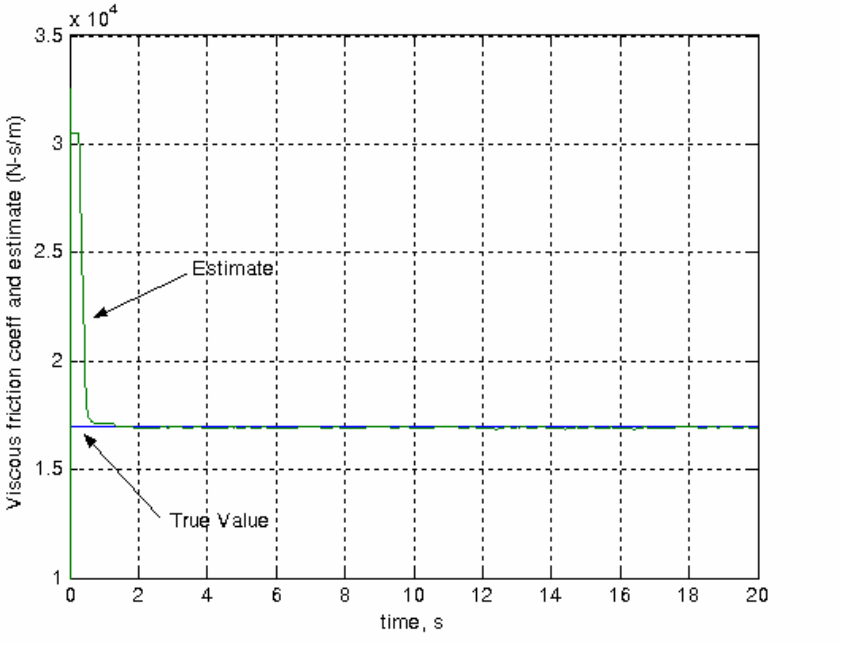

Fig. 5.2.1 Friction coefficient – True value and estimate (7-state EKF, nominal simulation)

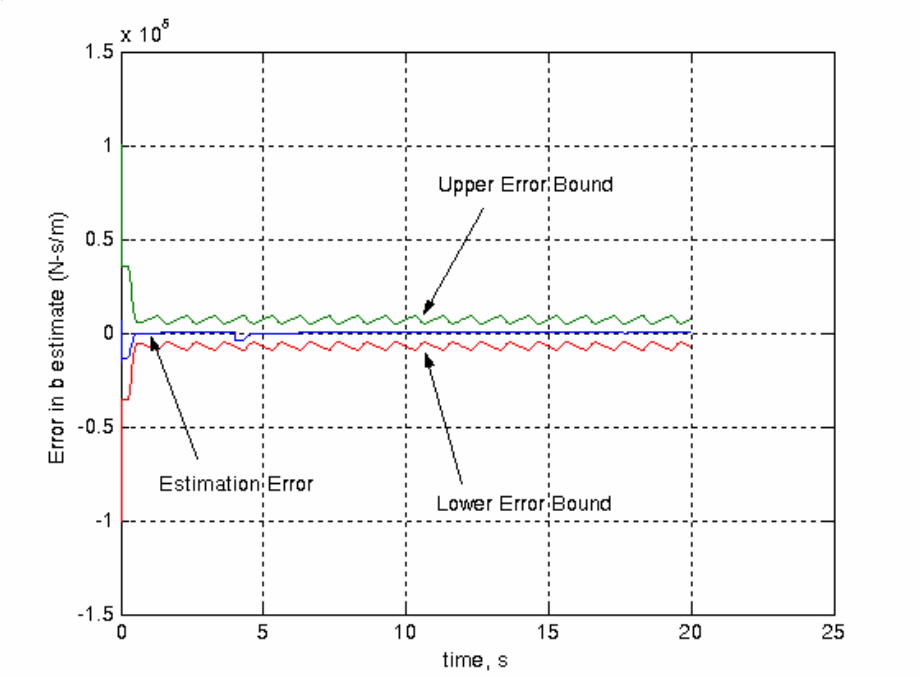

Fig. 5.2.2 Friction coefficient estimate error and error bounds (7-state EKF, nominal simulation)

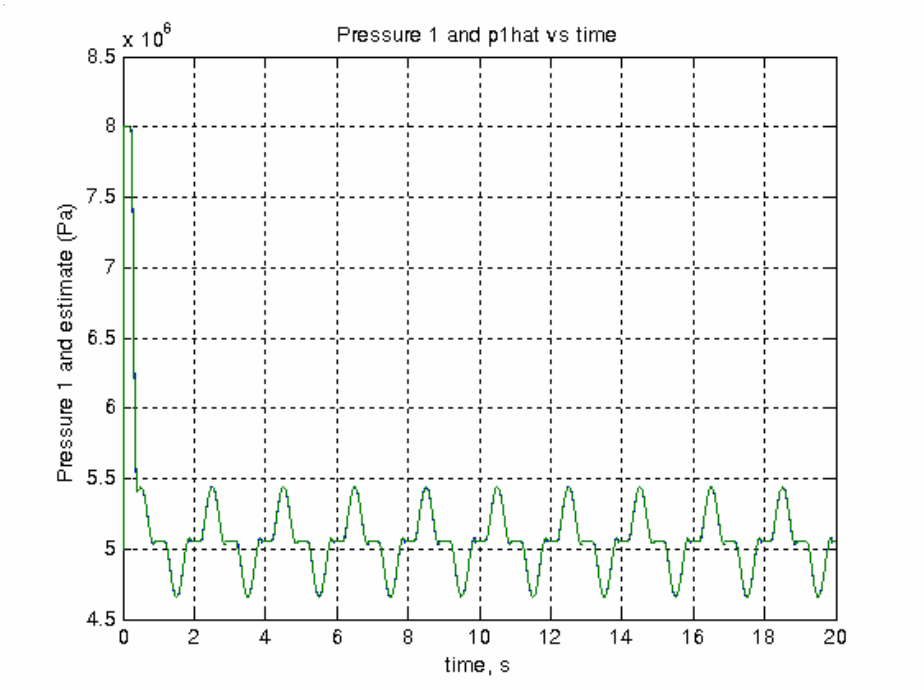

Fig. 5.2.3 Pressure 1 – True value and estimate (7-state EKF, nominal simulation)

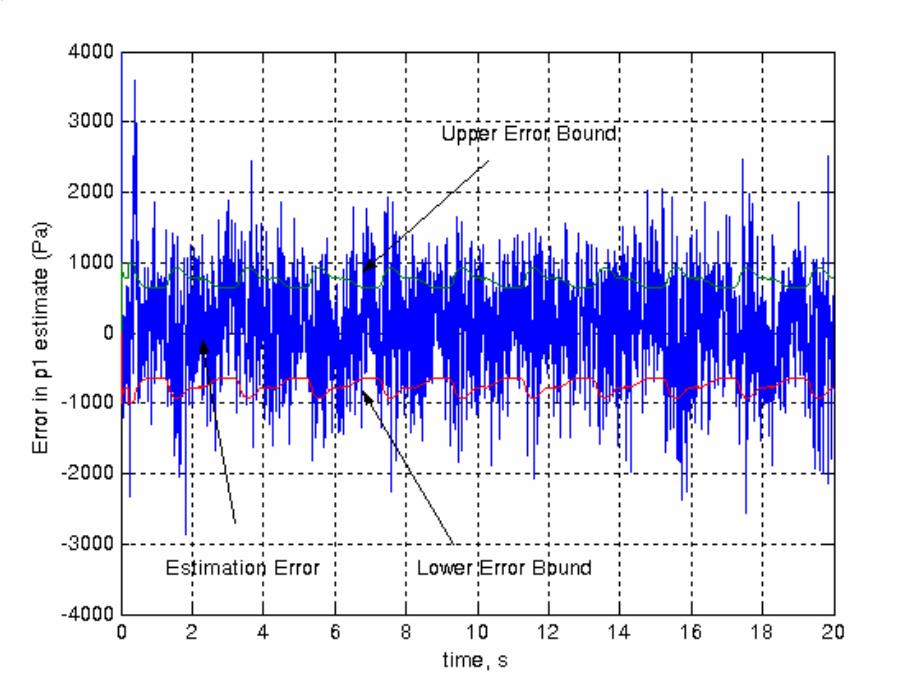

Fig. 5.2.4 Pressure 1 estimate error and error bounds (7-state EKF, nominal simulation)

The EKF has shown that it can directly estimate *b*, so we will now test its ability to detect faults that result in a change in friction coefficient. At 4 seconds into the simulation, the true value of *b* will decrease by 23.5% instantaneously. The EKF model has no knowledge of this fault. From the results in Figs. 5.2.5 and 5.2.6 it is apparent that the filter is able to track this type of fault *b*, as well over 68% of the error points lie within the error bounds. Similar to the no-fault estimate of friction coefficient (Fig. 5.2.1), the estimate needs a short time, about one second, to "catch up" to the true value before leaving the transient phase and tracking well. Then after the fault occurs, a similar time period is needed for the estimate to settle on the new post-fault value of *b*. It seems clear that this 7-state EKF model is effective as a detector of faults in viscous friction coefficient.

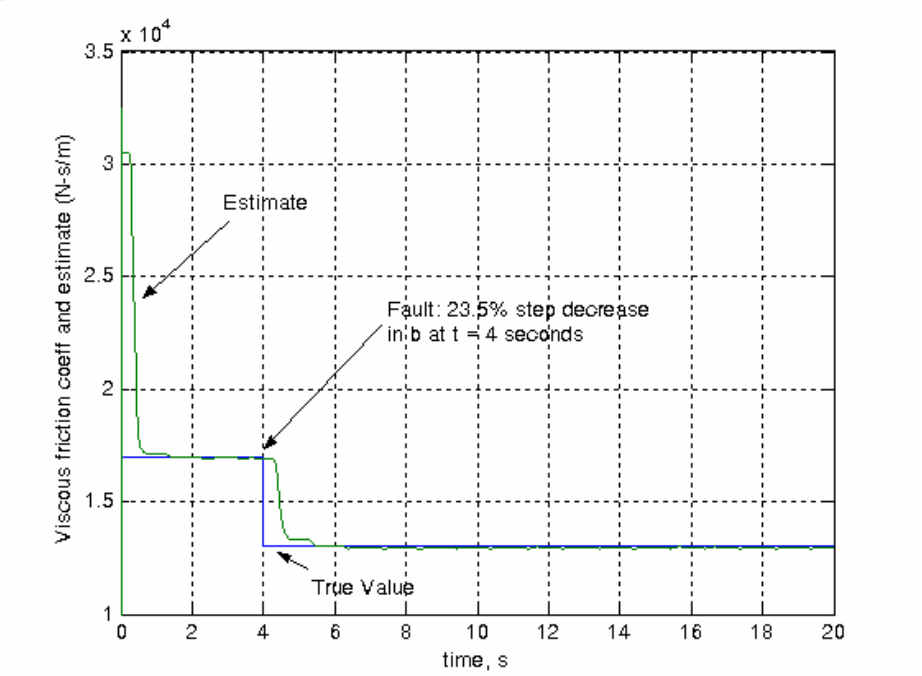

Fig. 5.2.5 Friction coefficient – True value and estimate (7-state EKF, 23.5% fault in *b* at t = 4 seconds)

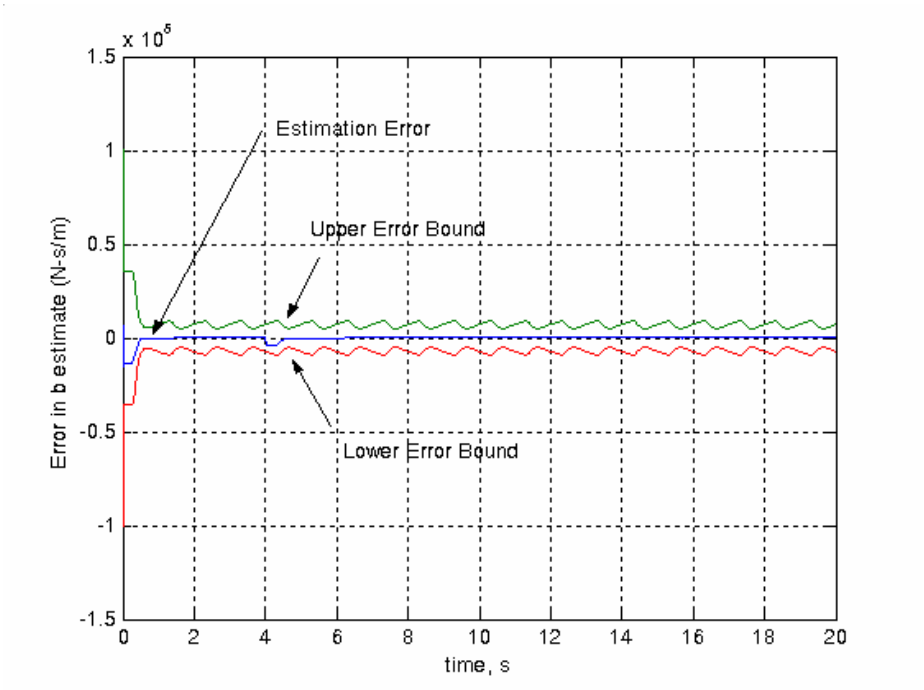

Fig. 5.2.6 Friction coefficient estimate error and error bounds (7-state EKF, fault: 23.5% decrease in *b* at t = 4 seconds)

5.3 Fluid Bulk Modulus

The eighth and final state added to this fault detection model is fluid bulk modulus, β. The same process described previously for adding friction coefficient as an augmented state will be used here. First, the tracking for the 8-state no-fault system will be checked. The "true" value for β is 1.57489(10^9) Pa, and the initial state estimate, $\hat{\beta}(0)$, is 1.5(10^9). Figures 5.3.1 and 5.3.2 indicate the 8-state EKF model appears to be effective as a state estimator. From Fig. 5.3.1, the steady-state tracking does not look as good as that of the other states, but 68% of the estimate error values lie within the $\pm 1\sigma$ error bounds shown in Fig. 5.3.2. Recall that, for a Gaussian distribution, about 68% of the data is $\pm 1\sigma$ from the mean. The noise is considered to be "white noise" in this case, which is Gaussian and has a zero mean. This indicates that the EKF is indeed performing well. Once again, the tracking performance of the six original physical states (P_1, P_2, x, $\dot{x}$, y, $\dot{y}$) and b, the other augmented state, does not differ from the results shown previously in Figs. 4.1.1-4.1.6 and Fig. 5.2.1. This affirms that the EKF still tracks well with the addition of a second augmented state to create an 8-state system.

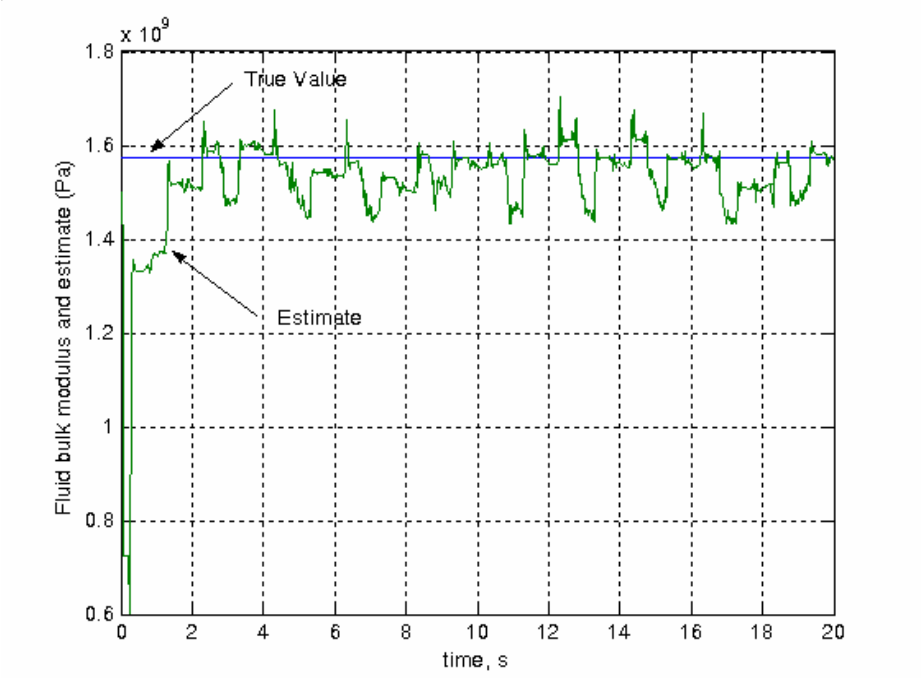

Fig. 5.3.1 Bulk modulus – True value and estimate (8-state EKF, nominal simulation)

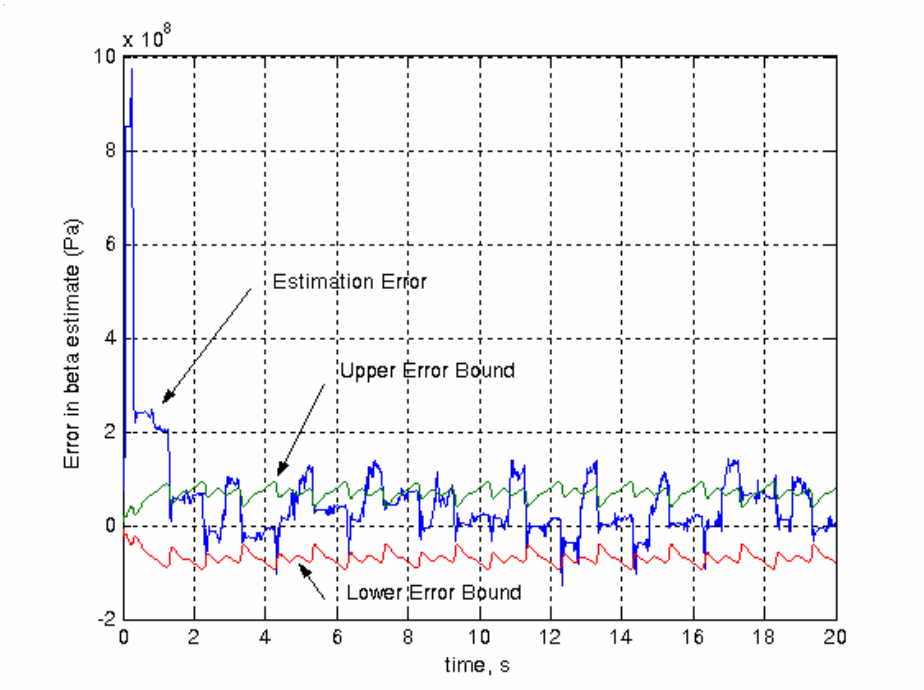

Fig. 5.3.2 Bulk modulus estimate error and error bounds (8-state EKF, nominal simulation)

As in the case with friction coefficient, a substantial change in fluid bulk modulus will be introduced mid-simulation to check the ability of the EKF, which has no knowledge of the existence of any faults in the truth model, to detect faults in β. At 12 seconds into the simulation, the true value of β will instantaneously decrease to 60% of its original value. This type of change in bulk modulus occurs with the presence of 1% entrained air. The results of the fault are seen in Figs. 5.3.3 and 5.3.4. Figure 5.3.3 shows that the EKF detects the change in β and arrives upon the post-fault value very quickly. It is noted that in Fig. 5.3.4, except for the unsurprising deviation at the occurrence of the fault, around 68% of the estimate error signal lies within its anticipated 1-σ error bounds. Although the fault at 12 seconds causes some transient error, the steady-state tracking remains acceptable for bulk modulus.

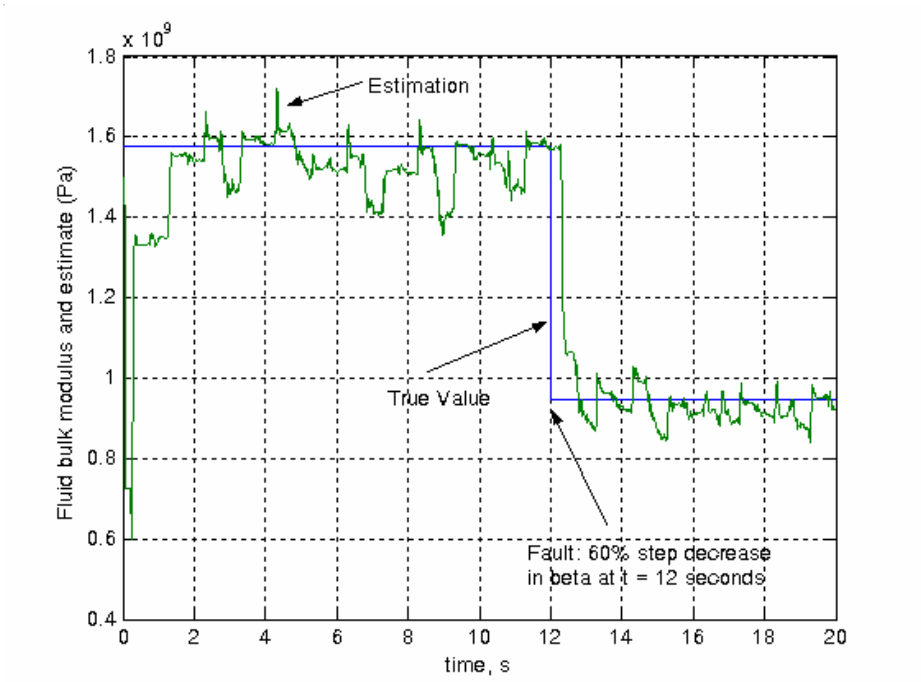

Fig. 5.3.3 Bulk modulus – True value and estimate (8-state EKF, 60% fault in β at t = 12 seconds)

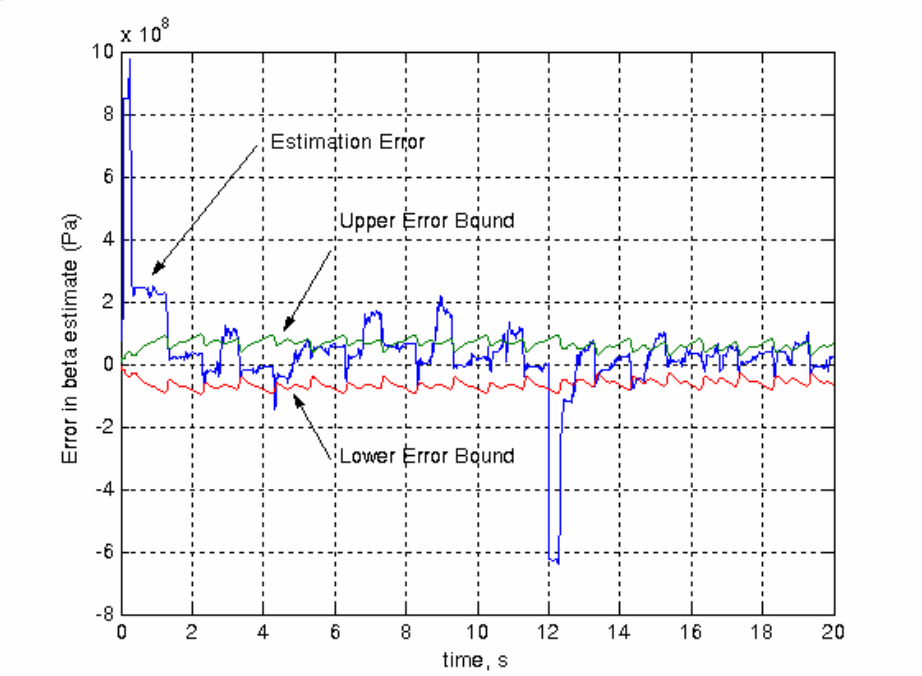

Fig. 5.3.4 Bulk modulus estimate error and error bounds (8-state EKF, 60% fault in β at t = 12 seconds)

5.4 External Leakage

Another type of fault very common in hydraulic systems is the leakage of hydraulic fluids from a pressure chamber, whether it be internal leakage across the cylinder to the low pressure side, or external leakage out of the system entirely. Both of these leakage flowrates are shown in the model schematic in Fig. 2.1.1. The first unmodeled fault to be examined is external leakage. Leaked flow is modeled as a leakage coefficient, k_{el} with units of m^3/Pa-s multiplied by a pressure difference, as seen in Eq. (5.4.1).

$$Q_{leak} = k_{el}(P - P_0) \tag{5.4.1}$$

In the case of external leakage, P_0 is atmospheric pressure.

Unlike the previous examples of friction coefficient and fluid bulk modulus, it is not feasible to directly estimate leakage coefficients because they are such small numbers, usually on the order of 10^{-12} m^3/Pa-s. There is such a large difference in order between leakage coefficients and the other states (for example, around 20 orders of magnitude difference with bulk modulus) that this EKF simply cannot estimate and track leakage coefficients if they were included as additional augmented states due to numerical difficulties. Instead, error residual data from the EKF will be used to indirectly detect leakages. Recall that the error residual is the difference between a sensor measurement and its corresponding state estimate, given in Eq. (5.4.2).

$$\mathbf{r} = \mathbf{y} - C\hat{\mathbf{x}} \tag{5.4.2}$$

Because only three states are measured, P_1, P_2, and x, $\boldsymbol{r}$ contains information relating to those states only. In the absence of a system fault, the error residuals should be nearly zero. Because the measurements are subjected to white noise, which is equally positive and negative and also has a zero mean, an error residual plot of a nominal simulation resembles a white noise plot, as seen in Fig. 5.4.1.

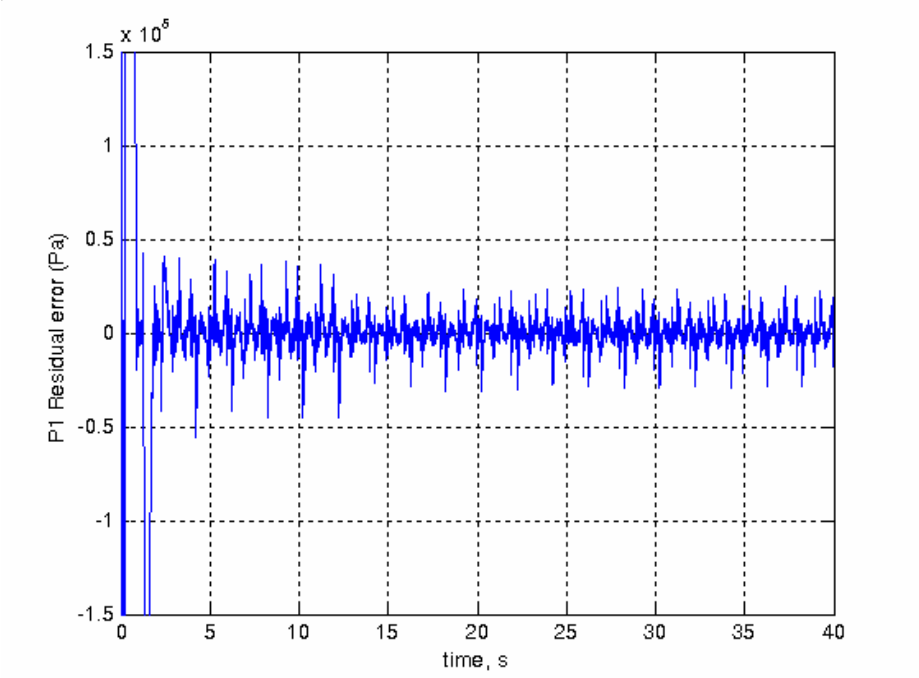

Fig. 5.4.1 Error residual for pressure 1 (8-state EKF, nominal simulation)

Using error residual data is an indirect approach to fault detection because it will reveal unmodeled faults. In this case, the possibility of leakage is not modeled by the EKF, so it cannot possibly have any knowledge of the existence of a leakage fault. So rather than directly estimating leakage, such as was done previously with b and β, the error residual data will be paramount in indicating the presence of a fault. Because r is the difference between a state estimate and its measurement, it should grow large when a fault is present and assume a value near zero otherwise. In order to make faults more apparent, some manipulation of the error residual is needed. The mean value will be used, because that is easier to monitor than a change in magnitude of a white noise signal, such as is shown in Fig. 5.4.1. But rather than a regular mean, it is appropriate to use a running average, so the error residual average is not biased by a relatively large amount of pre-fault data, making it difficult to determine the occurrence of a fault. And finally, because r resembles white noise, it has a zero mean, so the absolute value of the error

residual data will be used. This should provide a positive mean that will assume a value near zero for a nominal simulation and grow larger with the occurrence of a fault. These corrections are shown in Eq. (5.4.3):

$$r_{avg} = \frac{\sum_{i=k-n}^{k} |r_i|}{n} \tag{5.4.3}$$

where n is the window size of the average. For this simulation, the window size is a 4 second span, or, twice the period of the input function. Figure 5.4.2 shows the running average of the error residual data for a nominal simulation. Because the state estimates are initially very bad, the error residuals exhibit a very large spike before settling out to a nearly constant value. By neglecting the initial transient spike, the value of the error residual average can be seen in Fig. 5.4.3. For all future trials, the running average will be artificially held to zero for the first 5 seconds of the simulation to prevent the initial transient phase from skewing the results. Notice that the steady-state value is "small," but not zero. Again, this is because the average of the absolute value of r_i is being used, not just the mean of r_i. So instead of a zero mean, a user should look for the error residual value described by Eq. 5.4.3 to be "flat," such as in Fig. 5.4.3, to signify a good estimation process. A different type of error residual profile indicates the presence of an unmodeled fault.

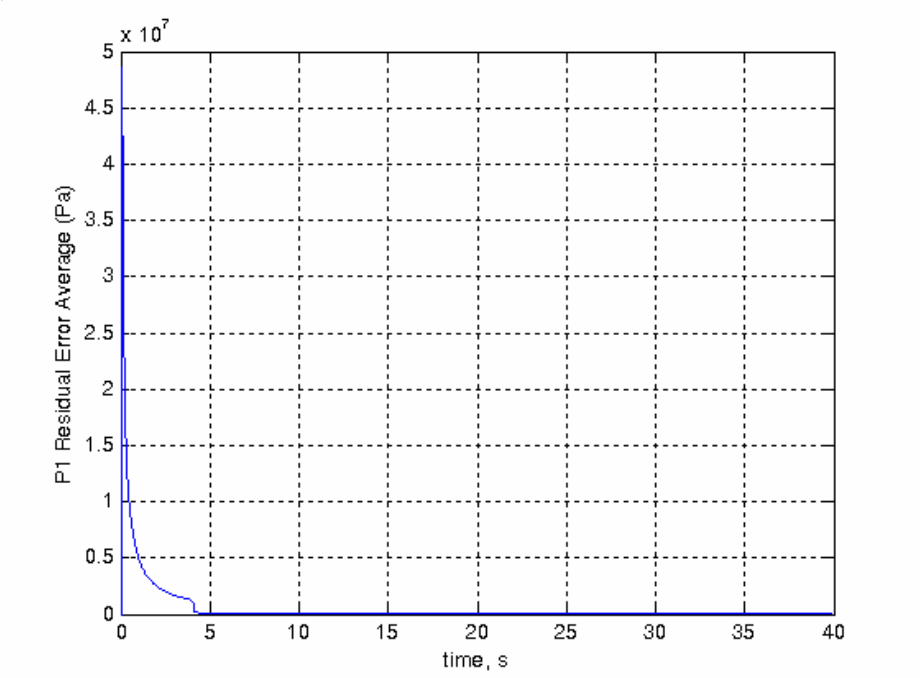

Fig. 5.4.2 Running average of error residual for pressure 1 (8-state EKF, nominal simulation)

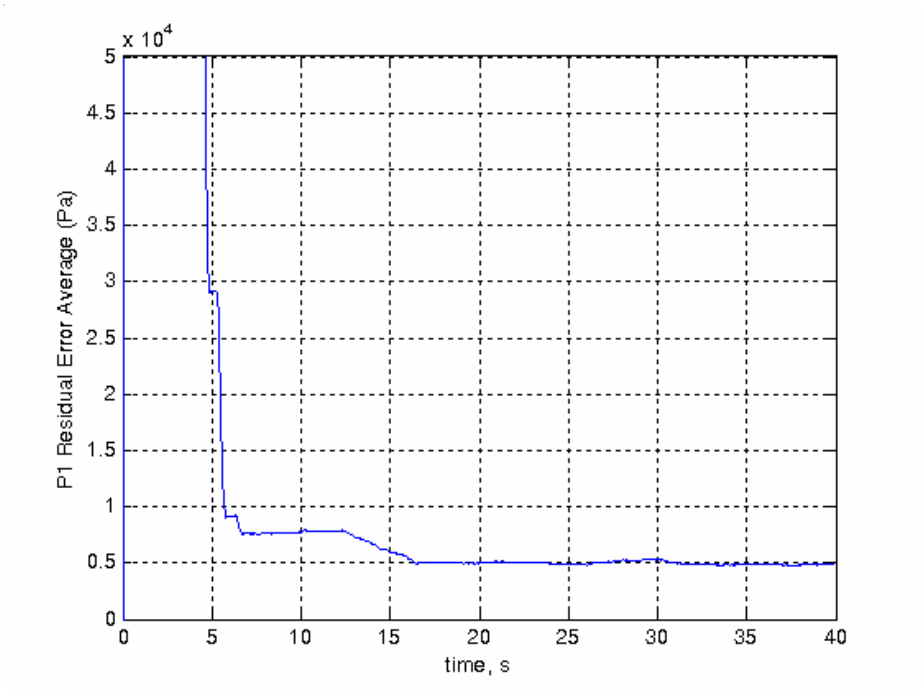

Fig. 5.4.3 Close-up view of running average of error residual for pressure 1 (8-state EKF, nominal simulation)

An external leakage will now be introduced into the system. At 16 seconds, an external leakage coefficient of $1.589(10^{-12})$ m^3/s-Pa is introduced into chamber 1, as seen in Fig. 5.4.4. It is clear that the pressure profile has been altered by the fault at 16 seconds, but it is not obvious until viewing the close-up view of P_1, shown in Fig. 5.4.5, that the state estimate also suffers. Not surprisingly, the estimate for P_1 becomes very poor at this point, and Fig. 5.4.6 confirms this, where it is apparent that at least 68% of the error data does not fall within the ±1-σ error bounds. It can be seen from Fig. 5.4.7 that the piston position drifts lower over time after the fault at 16 seconds, but the leak does not affect it enough to significantly impact the position estimate, as seen by the error bound plot in Fig. 5.4.8.

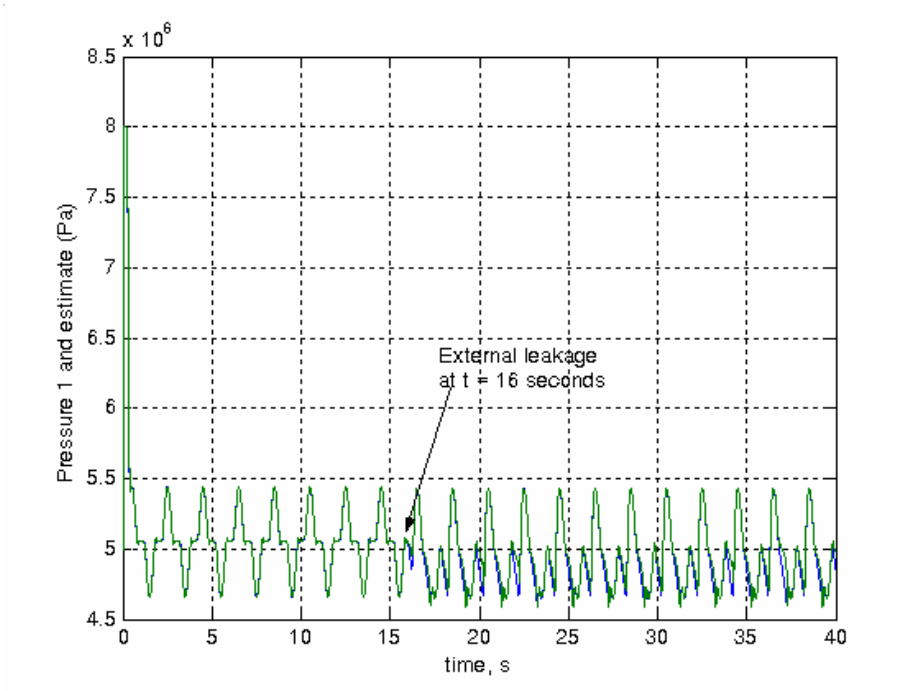

Fig. 5.4.4 Pressure 1 – True value and estimate (8-state EKF, external leakage at t = 16 seconds)

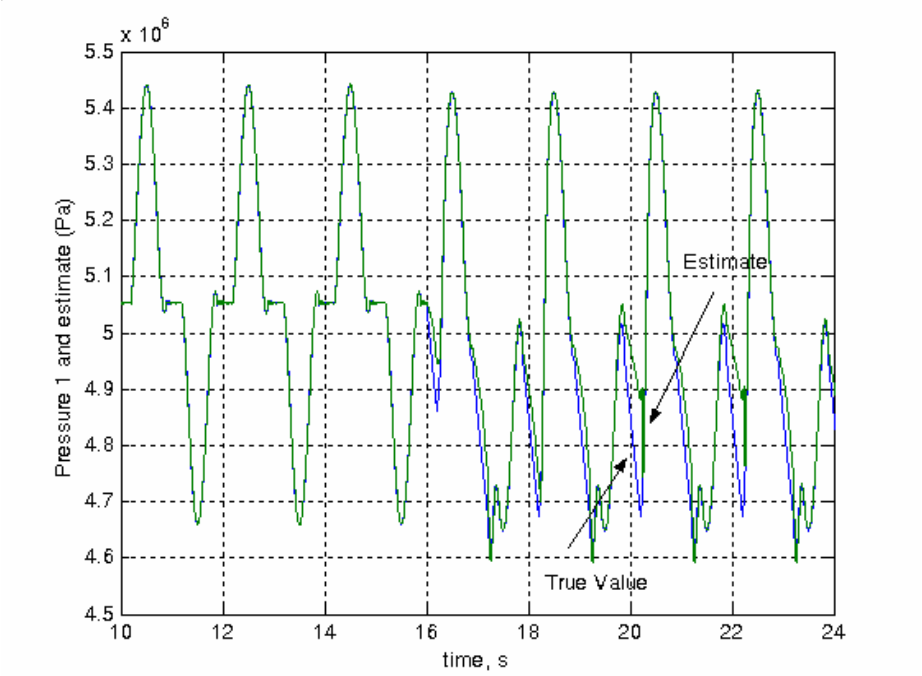

Fig. 5.4.5 Close-up view of pressure 1 – True value and estimate (8-state EKF, external leakage at t = 16 seconds)

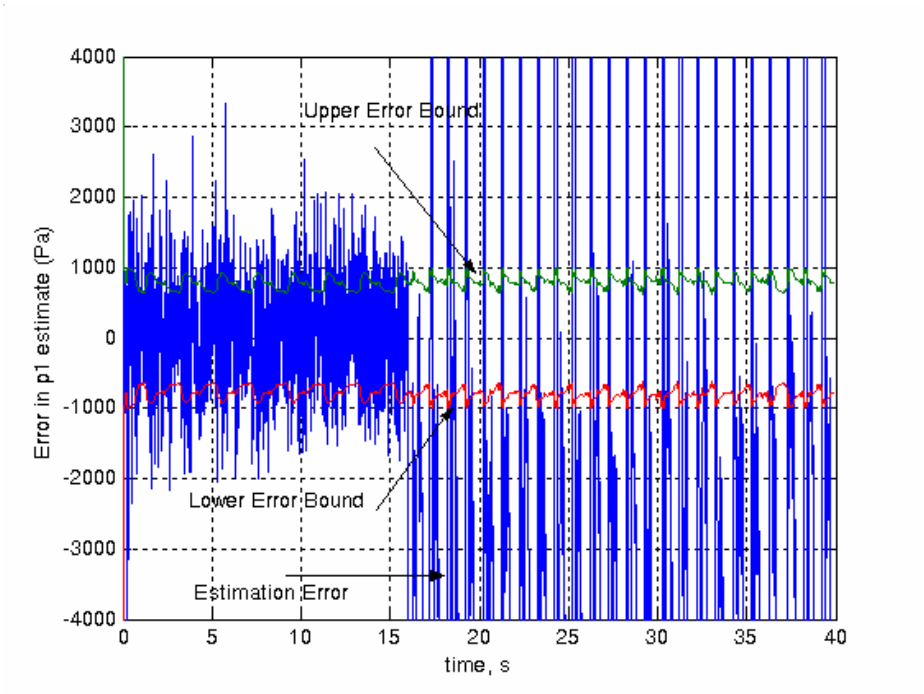

Fig. 5.4.6 Pressure 1 estimate error and error bounds (8-state EKF, external leakage at t = 16 seconds)

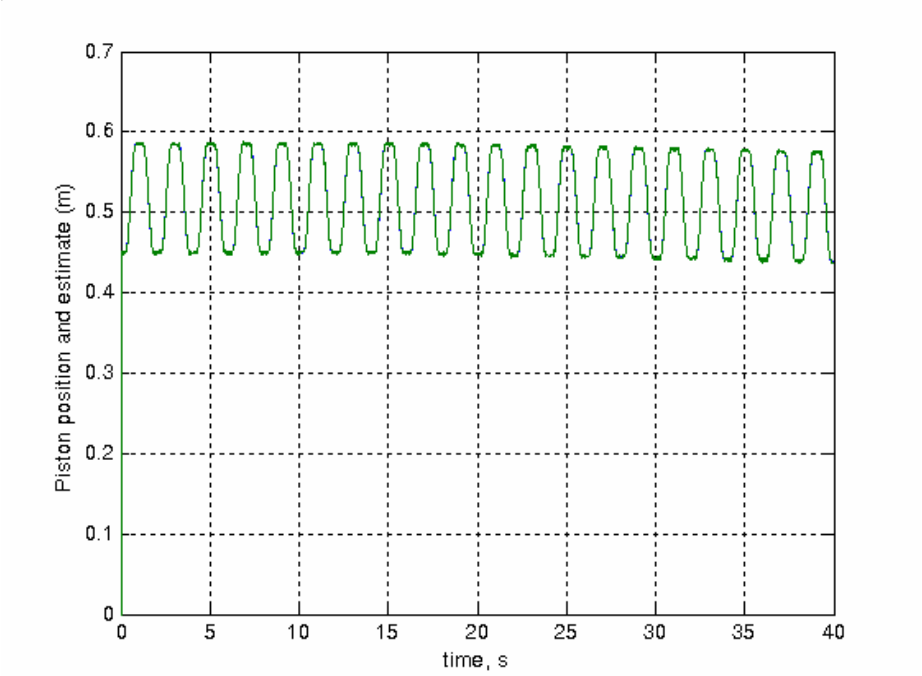

Fig. 5.4.7 Piston position -- True value and estimate (8-states EKF, external leakage at t = 16 seconds)

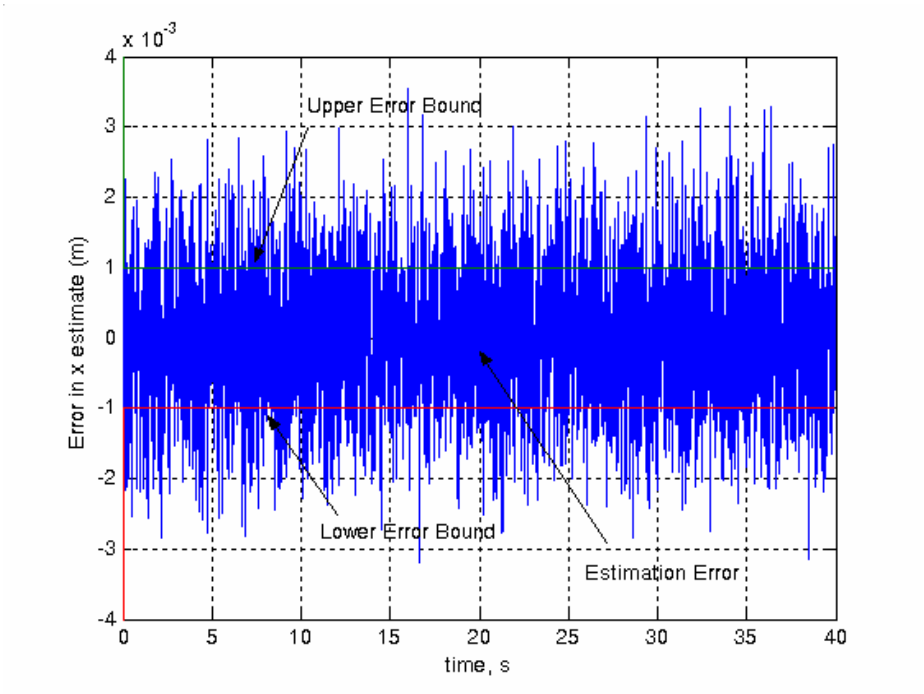

Fig. 5.4.8 Piston position estimate error and error bounds (8-state EKF, external leakage at t = 16 seconds)

It may seem that this data makes the presence of a fault quite apparent, making the use of error residual data redundant. Unfortunately, this information is only available with access to all of the "true" simulation data. This is most likely not the case for the vast majority of potential on-site applications for this fault detection method. Therefore, these types of error bound plots, such as Figs. 5.4.6 and 5.4.8, are useful for off-line validation of the EKF model, but not for actually indicating the presence of faults.

This external leakage fault is also apparent from the error residual data for P_1, which can be found in Fig. 5.4.9. The running average holds near zero until the fault occurs, and then very clearly deviates to a non-zero value, indicating the fault has been detected by the EKF. The running average of the error residual for piston position can be seen in Fig. 5.4.10. Although any deterioration of the piston position estimate due to the fault cannot be detected through visual inspection, the error residual data indicate the estimate did suffer.

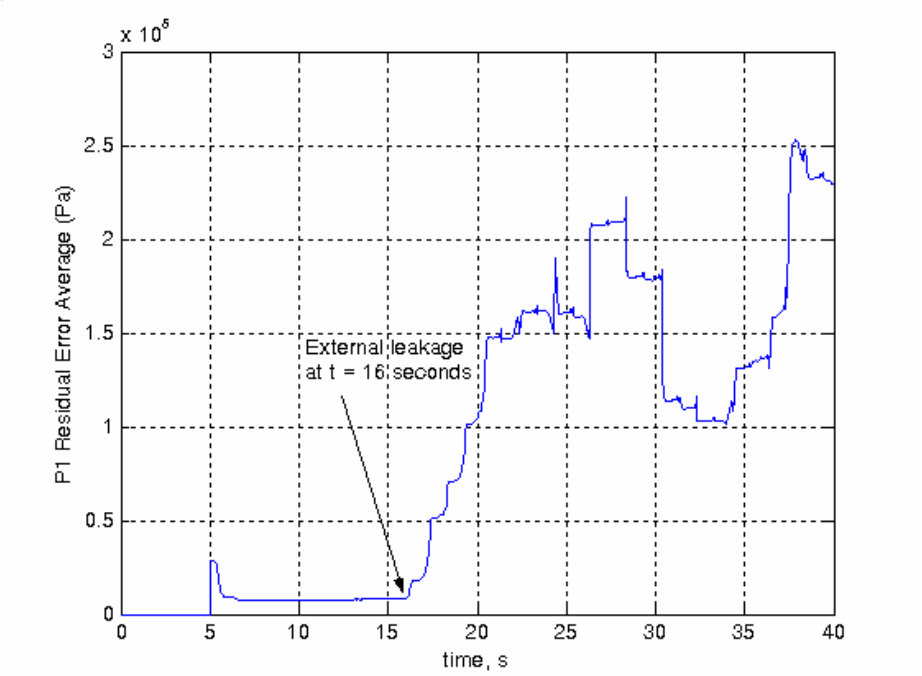

Fig. 5.4.9 Running average of error residual for pressure 1 (8-state EKF, external leakage at t = 16 seconds)

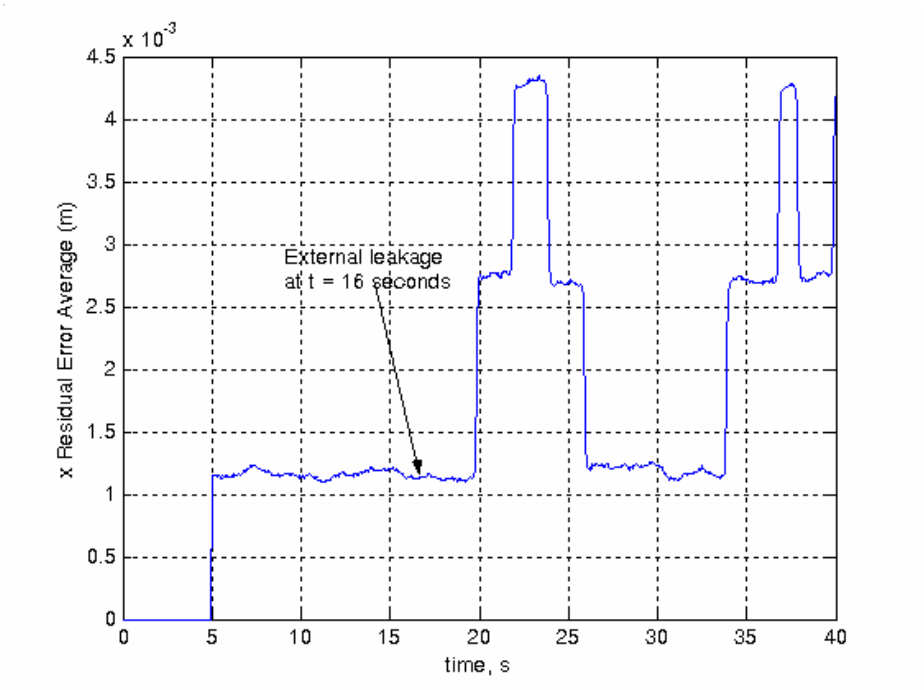

Fig. 5.4.10 Running average of error residual for piston position (8-state EKF, external leakage at t = 16 seconds)

It should be remembered that this fault detection method is not the same as that used previously for faults in friction coefficient and fluid bulk modulus. Those parameters were added to the state-space representation as augmented states, and directly estimated by the EKF to indicate the presence of a fault. This is an indirect method for fault detection; rather than directly estimating a system error, this method uses the discrepancy between a state measurement and its EKF estimate to signal the presence of an unmodeled fault.

5.5 Internal Leakage

Besides external leakage, there is also interest in detecting internal leakage between cylinder chambers. Internal leakage is characterized by the passage of hydraulic fluid from the high-pressure chamber to the low-pressure chamber across the cylinder. The leaked flow is similar to that of Eq. (5.1), but atmospheric pressure, P_0, is replaced by the lower of the two cylinder chamber pressures as can be seen in Eq. (5.5.1),

$$Q_{leak} = k_{il}\Delta P$$
$$\Delta P = \begin{cases} P_1 - P_2 \quad if \quad P_1 > P_2 \\ P_2 - P_1 \quad if \quad P_2 > P_1 \end{cases} \tag{5.5.1}$$

Like in the previous cases, the simulation is run for a time to allow the transients to settle, and then a fault is introduced into the truth model. At 16 seconds, an internal leakage with a coefficient of $11.503(10^{-12})$ m^3/s-Pa is instituted. Once again, the initial transient errors have been manually set to zero to give a clear view of the impact of a fault on the error residual. The results are shown in Figs. 5.5.1-5.5.3. As in the case of external leakage, it is obvious that 68% of the error signal data does not fall within the

±1-σ error bounds, clearly indicating a fault. Although the tracking and the estimation errors do not appear by inspection to be significantly better than those from the external leakage trial, the impact of an internal leakage on the system is roughly 2-3 times less severe than that of an external leakage. Figure 5.5.3 shows the running average of the P_1 error residual clearly indicates a fault is detected, but notice the post-fault value is smaller than on the external leakage error residual plots. The P_2 error residual data, which is not shown, reflects the same results as those shown for P_1. It is apparent that this EKF fault detection scheme does indeed detect the presence of internal leakages.

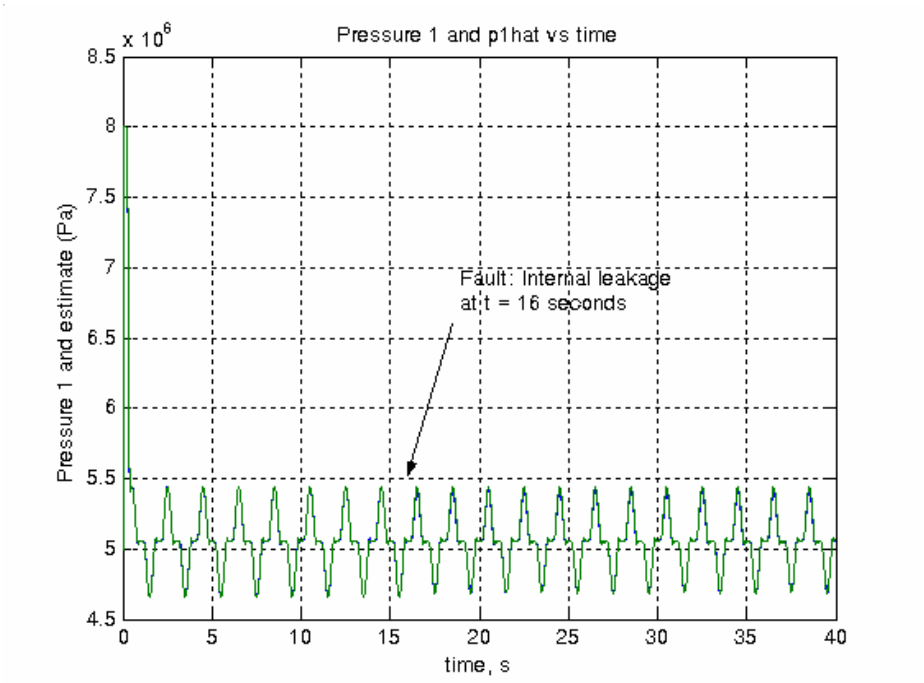

Fig. 5.5.1 Pressure 1 – True value and estimate (8-state EKF, internal leakage at t = 16 seconds)

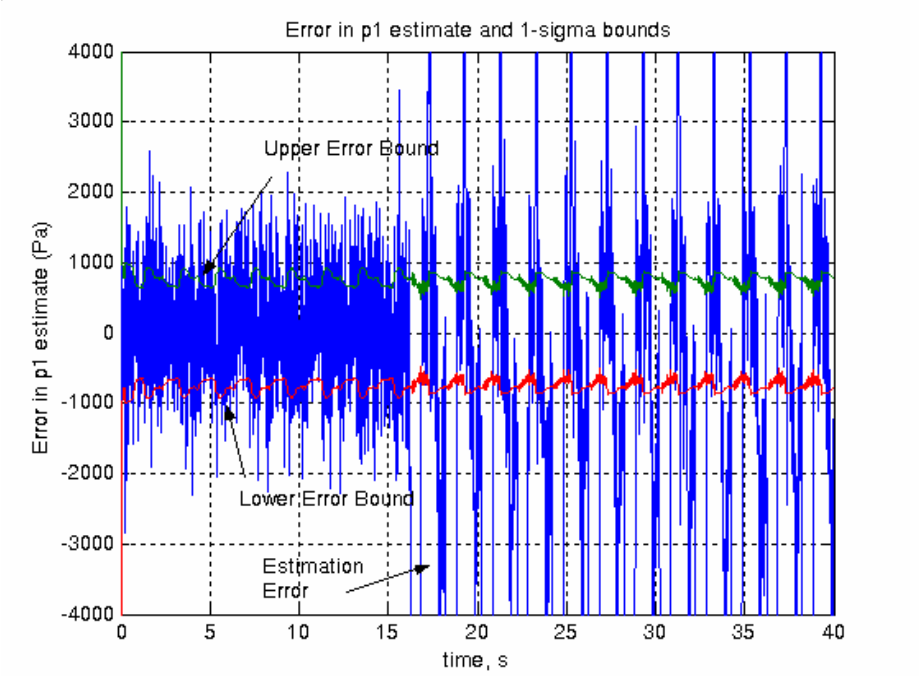

Fig. 5.5.2 Pressure 1 estimate error and error bounds (8-state EKF, internal leakage at t = 16 seconds)

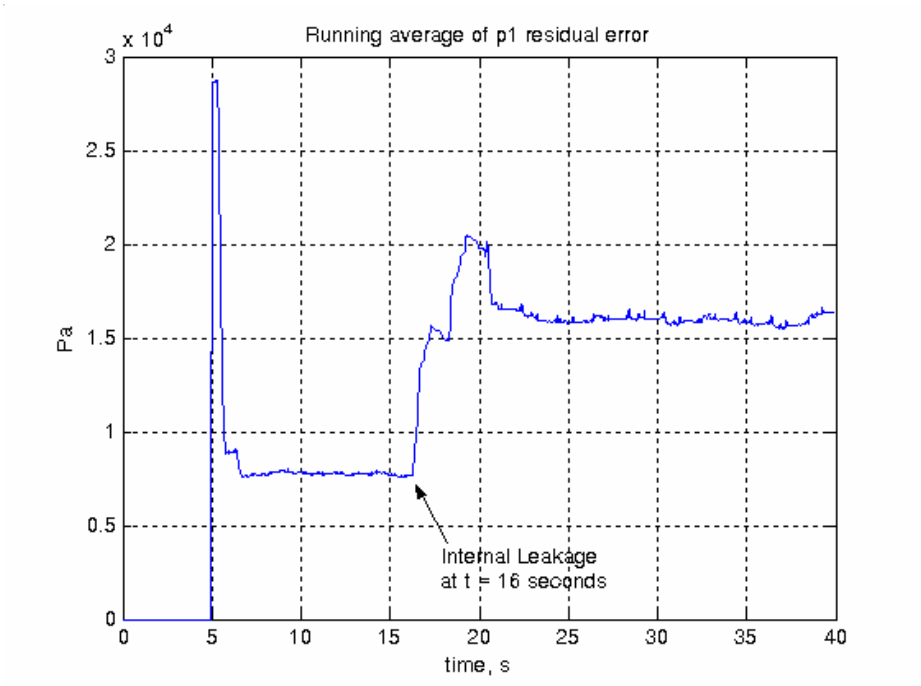

Fig. 5.5.3 Running average of error residual for pressure 1 (8-state EKF, internal leakage at t = 16 seconds)

Chapter 6

SUMMARY AND CONCLUSIONS

6.1 Summary

A scheme for detecting various types of faults in a hydraulic actuator system was desired. The method described within this work employs an extended Kalman filter as a state estimator. An EKF-type state observer has two substantial advantages over other traditional state observers. Firstly, the EKF uses a recursive algorithm, eliminating the need for data storage. This is especially useful for off-road hydraulic equipment, where large amounts of computer storage are commonly not available or convenient. Additionally, the EKF algorithm contains an error model which accounts for process and measurement noise, two quantities that frequently have significant impact in large hydraulic machines.

The EKF uses two different techniques for determining the presence of a fault, one direct and the other indirect. The direct fault detection method involves including system parameters as augmented states and tracking changes in the state estimates for those augmented states after introducing a fault in the truth simulation. This technique is considered to be a direct fault detection method because the fault itself (a parametric change) is estimated by the EKF.

The indirect method uses error residual data to determine unmodeled system faults. In this work, the unmodeled faults are external and internal leakages. The error residuals are the difference between a state's measurement and its estimate. To make faults more apparent, the running average of the absolute value of the error residuals is

analyzed. In the absence of a fault, the error residual data profile should display a flat line with a value near zero. When a fault occurs, the error residual becomes larger in size and irregular in profile, indicating that a fault has been flagged by the EKF.

6.2 Conclusions

The results presented in Chapter 5 indicate that the EKF scheme presented here proves to be an effective fault detection tool in this hydraulic actuator system. In the case of fault detection via the estimate of augmented states, it was found that the EKF tracks faults accurately and promptly. This claim of good tracking is confirmed by the EKF embedded diagnostic tool, the $\pm 1\text{-}\sigma$ error bounds derived from the error covariance matrix. When the EKF is performing well, around 68% of a state's error signal should lie within those bounds, which was found to be the case for all of the augmented state faults presented here.

Similarly, it was found that the EKF is useful in indicating the presence of unmodeled faults, such as leakages. The running average of the error residual maintained a near-constant value close to zero until a fault occurs. After a fault takes place, the error residual data profile dramatically changes, making the existence of a fault apparent to an operator.

6.3 Future Work

There is much room for expansion on this work. The system model used here is extremely simple. A more complicated and realistic model would be instructive in proving the effectiveness of this EKF fault detection scheme. This applies to several

areas of the system model, notably, adding a pump model for the supply pressure and also by providing a more realistic cylinder friction model. Another natural hardware extension is the inclusion of a load cell on the cylinder. This would be a simple addition, and would add one more physical state to the baseline model. Additionally, authentic operator stick input may be more useful than the sinusoid input signal used here. There is a possibility that including irregular input will damage state estimates, but it is expected that this EKF scheme will still perform well. Because of this uncertainty, the addition of user input is especially valuable for model validation. And perhaps the most important possible future development is the hardware validation of this fault detection scheme. Until the fault detection algorithm is loaded on a machine and tested, much will remain uncertain.

Appendix A

The EKF matrices requiring user input are provided here. C is the output matrix for the three measurements, P_1, P_2, and x. W and V are the sensor and process noise matrices, respectively. The terms making up these two matrices have the structure of covariance (σ^2) terms. P^- is the initial error covariance matrix upon entering the EKF loop. This matrix is then updated and evolves according to the EKF algorithm.

$$C = \begin{bmatrix} 1 & 0 & 0 & 0 & 0 & 0 & 0 & 0 \\ 0 & 1 & 0 & 0 & 0 & 0 & 0 & 0 \\ 0 & 0 & 1 & 0 & 0 & 0 & 0 & 0 \end{bmatrix}$$

$$W = \begin{bmatrix} 10^{6} & 0 & 0 \\ 0 & 10^{6} & 0 \\ 0 & 0 & 10^{-6} \end{bmatrix}$$

$$V = \begin{bmatrix} 10^{2} & 0 & 0 & 0 & 0 & 0 & 0 & 0 \\ 0 & 10^{2} & 0 & 0 & 0 & 0 & 0 & 0 \\ 0 & 0 & 10^{-3} & 0 & 0 & 0 & 0 & 0 \\ 0 & 0 & 0 & 10^{-2} & 0 & 0 & 0 & 0 \\ 0 & 0 & 0 & 0 & 10^{-10} & 0 & 0 & 0 \\ 0 & 0 & 0 & 0 & 0 & 10^{-10} & 0 & 0 \\ 0 & 0 & 0 & 0 & 0 & 0 & 10^{6} & 0 \\ 0 & 0 & 0 & 0 & 0 & 0 & 0 & 10^{7} \end{bmatrix}$$

$$P^{-} = \begin{bmatrix} 10^{6} & 0 & 0 & 0 & 0 & 0 & 0 & 0 \\ 0 & 10^{6} & 0 & 0 & 0 & 0 & 0 & 0 \\ 0 & 0 & 10^{4} & 0 & 0 & 0 & 0 & 0 \\ 0 & 0 & 0 & 10^{4} & 0 & 0 & 0 & 0 \\ 0 & 0 & 0 & 0 & 10^{4} & 0 & 0 & 0 \\ 0 & 0 & 0 & 0 & 0 & 10^{4} & 0 & 0 \\ 0 & 0 & 0 & 0 & 0 & 0 & 10^{10} & 0 \\ 0 & 0 & 0 & 0 & 0 & 0 & 0 & 10^{7} \end{bmatrix}$$

REFERENCES

[1] An, L. and Sepehri, N., 2005, "Hydraulic Actuator Leakage Fault Detection Using Extended Kalman Filter," International Journal of Fluid Power, **6**, pp. 41-51.

[2] An, L. and Sepehri, N., 2003, "Hydraulic Actuator Circuit Fault Detection using Extended Kalman Filter," Proceedings of American Control Conference, **5**, pp. 4261-4266.

[3] Chinniah, Y., Burton, R., and Habibi, S., 2003, "Viscous Damping Coefficient and Effective Bulk Modulus Estimation in a High Performance Hydrostatic Actuator Using Extended Kalman Filter," International Journal of Fluid Power, **4**, pp. 27-34.

[4] Song, R., and Sepehri, N., 2002, "Fault Detection and Isolation in Fluid Power Systems Using a Parametric Estimation Method," IEEE CCECE Canadian Conference on Electrical and Computer Engineering, **1**, pp. 144-149.

[5] Shields, D. N., Ashton, S. A., and Daley, S., 2001, "Robust Fault Detection Observers for Nonlinear Polynomial Systems," International Journal of Systems Science, **32**, pp. 723-737.

[6] Hajiyev, C. M., Caliskan, F., 1999, "Fault Detection in Flight Control Systems Based on the Generalized Variance of the Kalman Filter Innovation Sequence," Proceedings of the American Control Conference, **1**, pp. 109-113.

[7] Venkatasubramanian, V., Rengaswamy, R., Yin, K., Kavuri, S. N., 2003, "A Review of Process Fault Detection and Diagnosis Part 1: Quantitative Model-based Methods," Computers and Chemical Engineering, **27**, pp. 293-311.

[8] Frank, P. M., 1994, "On-line Fault Detection in Uncertain Nonlinear Systems Using Diagnostic Observers: A Survey," International Journal of System Science, **25**, pp. 2129-2154.

[9] Chow, E. Y., Willsky, A. S., 1984, "Analytical Redundancy and the Design of Robust Failure Detection Systems," IEEE Transactions on Automatic Control, **29(7)**, pp. 603-614.

[10] De Parsis, C., Isidori, A., 2001, "A Geometric Approach to Nonlinear Fault Detection and Isolation," IEEE Transactions on Automatic Control, **46(6)**, pp. 865.

[11] Brown, R. G., 1983, *Introduction to Random Signal Analysis and Kalman Filtering*, John Wiley and Sons, New York.

[12] Manring, N. D., 2005, *Hydraulic Control Systems*, John Wiley and Sons, New Jersey.